ACS OMEGA

Open Access

http://pubs.acs.org/journal/acsodf

Article

Discovery of Palazestrant (OP-1250), a Potent and Orally Bioavailable Complete Estrogen Receptor Antagonist (CERAN) and Selective Estrogen Receptor Degrader (SERD)

Raymond A. Ng,* Susanna Barratt, Alison Parisian, Gopinath S. Palanisamy, Samiron Phukan, Richard Sun, Brandon Robello, Guadalupe Peña, Judevin Sapugay, David Yeghikyan, Chenbo Wang, Samir Satish Kher, Srinivasan Thangathirupathy, Robert Millikin, Guijun Yu, Teruki Watanabe, Fei Zhou, Brian Rich, Alexis Duncan, Samuel E. Andersen, Reena Chawla, David R. Zak, Dirk A. Heerding, Brian R. Hearn, Geoffrey Greene, Cyrus L. Harmon, Leslie Hodges-Gallagher, Peter J. Kushner, Sean W. Fanning, and David C. Myles*

Cite This: *ACS Omega* 2025, 10, 22685−22700

Read Online

ACCESS | Metrics & More | Article Recommendations | Supporting Information

ABSTRACT: Metastatic breast cancer (mBC) is a leading cause of cancer death in women. Most breast cancer patients are administered estrogen-receptor-targeted endocrine therapies to treat or prevent progressive metastatic disease. Development of endocrine resistance through acquisition of mutations in the estrogen receptor gene, *ESR1*, that constitutively activate the estrogen receptor leads to relapse. Complete antagonism of both WT and mutant *ESR1* (*mutESR1*) with an oral therapeutic that persistently antagonizes ER-driven oncogenic transcriptional activities is a requirement for efficacy. Here, we describe our discovery of the investigational drug OP-1250 (palazestrant). OP-1250 is a potent complete estrogen receptor antagonist (CERAN) and selective estrogen receptor degrader (SERD) that is active in both WT and *mutESR1* breast cancer tumors. OP-1250's effective induction of tumor regression either as a single agent or in combination with a CDK4/6 inhibitor has led to the rapid advancement of this compound into a Phase 3 clinical trial (OPERA-01).

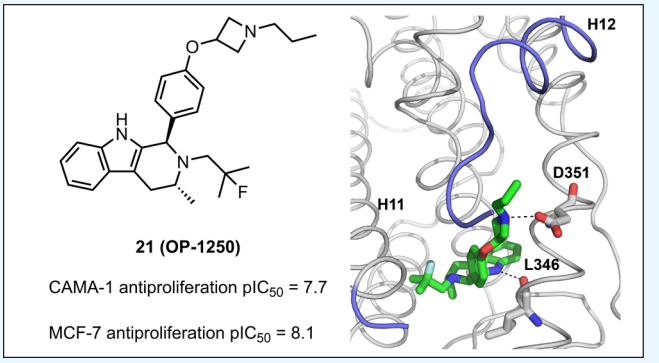

INTRODUCTION

Breast cancer is the second most common cause of cancer death in women worldwide after lung cancer.[1] In 2023, approximately 298,000 women in the U.S. were diagnosed with breast cancer. Around 80% of all breast cancers express estrogen receptor alpha (ER).[2] The transcriptional regulatory activities of ER occur via two activation functions (AF), AF1 and AF2 (Figure 1). Endogenous 17β-estradiol (E2) interacts with the ER ligand binding domain (LBD), leading to ER dimerization, ER binding to estrogen response elements, and the transcription of genes under the promotion of AF2. Transcription via AF1 in the N terminus is hormone-independent and can be promoted by a range of growth factors.[3] For complete inhibition of ER-driven transcription, both AF1 and AF2 must be blocked.[3a,b] In the absence of this complete blockade, AF1 is free to drive uncontrolled cell proliferation, tumor growth, and metastasis in ER+ breast cancers.

Current endocrine therapy (ET) options include aromatase inhibitors (AIs), selective estrogen modulators (SERMs), and selective estrogen receptor downregulators or degraders (SERDs) (Figure 2). AIs reduce the production of endogenous E2. However, prolonged use of AIs places selective pressure on the tumor that promotes the emergence of activating somatic *ESR1* mutations.[4] Tyr537 and Asp538 loci in the ligand-binding domain are two of the most common mutational hotspots. Tyr537Ser/Asn/Cys and Asp538Gly mutations enable estrogen-free constitutive transcriptional activity in the absence of E2 by stabilizing the receptor in the AF2 active conformation, thereby diminishing the effectiveness of AIs.[5] These mutations also reduce the binding affinity of ligands (both agonists and antagonists) to the LBD.

SERMs, such as tamoxifen **1a** and its active metabolite 4-hydroxytamoxifen **1b**, block only AF2 in the LBD,[3b] leaving

Received: December 13, 2024
Revised: May 6, 2025
Accepted: May 20, 2025
Published: May 29, 2025

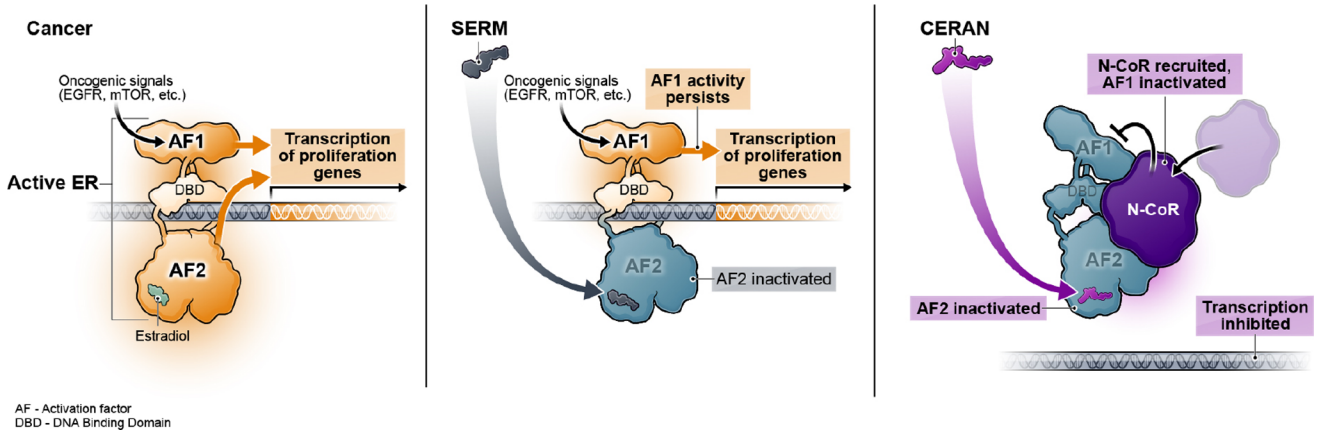

Figure 1. Complete estrogen receptor antagonist (CERAN) effectively blocks transcription mediated by both AF1 and AF2.

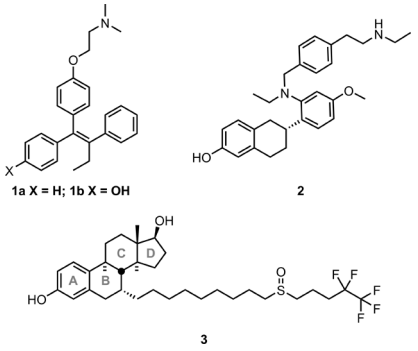

Figure 2. Example of SERM, tamoxifen **1a** and it is active metabolite, 4-hydroxytamoxifen (4OHT) **1b**, SERM/SERD elacestrant **2** and CERAN/SERD fulvestrant, (FULV) **3**.

AF1 free to stimulate tumor growth by activation through signaling from growth factor receptors such as mTOR, PI3K, MAPK, c-SRC, EGFR, FGFR, and IGFR (Figure 1, SERM). Failure to block AF1 drives increased expression of genes associated with cell cycle progression and proliferation.[3c] As a result, SERMs display both estrogenic and antiestrogenic profiles.

Elacestrant **2** (Orserdu, Figure 2), which exhibits a SERM profile[6,7] with modest SERD activity (Figure 12c), was recently approved for second and third-line treatment of mBC patients harboring Tyr537Ser and Asp538Gly *mutESR1*. However, elacestrant **2** showed only a modest effect in progression-free survival for *ESR1* WT patients.[8]

Fulvestrant **3** (Faslodex, Figure 2), a mainstay of first-line ET, competitively and potently inhibits binding of E2 to ER.[9] In contrast to 4-hydroxytamoxifen **1b**, fulvestrant **3** disrupts signaling by both AF1 and AF2, leading to complete antiestrogenic activity (Figure 1, CERAN). Additionally, fulvestrant **3** induces ER proteasomal degradation and is a SERD. The FIRST study[10] demonstrated that fulvestrant **3** (500 mg), a CERAN/SERD, was clinically superior to anastrozole (1 mg). The effectiveness of fulvestrant **3** is, however, limited by its poor pharmacokinetic (PK) properties. Fulvestrant **3** must be administered intramuscularly at 2 × 250 mg doses monthly. Drug exposure, even at this highest administrable dose, is not sufficient to completely abrogate ER signaling in the tumor.[11] The decreased ligand affinity of the activating mutant ER presents an even greater challenge for drugs, such as fulvestrant **3**, with limited exposure. Although fulvestrant **3** is considered a SERD, antagonism of ER precedes degradation,[12] and full ER degradation is not observed.[6] In the presence of fulvestrant **3**, ER is modified with small-ubiquitin-related modifiers 1/2/3 (SUMO1/2/3), which reduces the ability of ER to bind to estrogen response elements on chromatin.[13] Levels of ligand-induced SUMOylation of ER have been shown to correlate with higher antagonist activity of fulvestrant **3** (CERAN/SERD) as compared to elacestrant **2** (SERM/SERD) and 4-hydroxytamoxifen **1b** (SERM).[12] Additionally, the degradation of ER by fulvestrant is not required for antagonist efficacy.[14]

SERDs elicit proteasomal degradation of ERα to varying degrees. In addition to the monovalent degrader activity, an ER ligand also displays functional activity on the available estrogen receptor. There are ER full agonist/SERDs (e.g., E2[15]), SERM/SERDs (e.g., elacestrant **2**, AZD9496[16] **4**), and CERAN/SERDs (e.g., fulvestrant **3**, camizestrant[17] **5**, giredestrant[18] **6**, GDC-0927[19] **7**, imlunestrant[20] **8**, and amcenestrant[21] **9** (Figures 2 and 3)). Unless degradation occurs quickly and the SERD degrades nearly all of the estrogen receptor, the ER antagonism rather than the ER degradation of the SERD will determine the degree of efficacy. As a strategy, we chose to focus our medicinal chemistry efforts on optimizing for full antagonist activity, regardless of efficacy from induced ER degradation. Although our investigational drug **21** was confirmed as a SERD (Figure 12) in addition to its CERAN activity, we will focus on the antagonist activity of compounds in this paper and refer to them as CERANs. Other groups[15−21] have focused on ER degradation as the primary metric for guiding medicinal chemistry programs, a strategy that has also led to the development of effective CERAN/SERDs. In addition to monovalent degraders, a bivalent degrader targeting ER has been advanced into the clinic by Arvinas.[22] The advancement of numerous CERAN/SERDs into clinical development emphasizes the significant unmet need for a next-generation orally bioavailable CERAN/SERD that is well tolerated and can treat all ER+ mBC patients.[23]

The combination of ET with a CDK4/6[24] inhibitor (palbociclib, ribociclib, or abemaciclib) is currently the standard-of-care (SOC) in the first-line setting for patients with (HR+/HER2-) mBC. Ribociclib is emerging as a leader among the CDK4/6 inhibitors. The driving force behind this shift in practice was the observation that ribociclib showed an overall survival (OS) benefit relative to other CDK4/6 inhibitors in combination with ET.[25] In spite of the promising

https://doi.org/10.1021/acsomega.4c11023
ACS Omega 2025, 10, 22685−22700

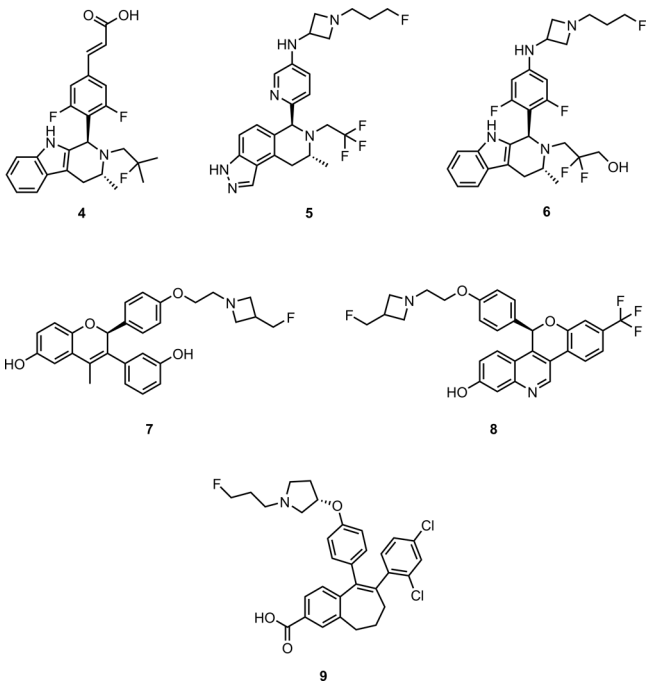

Figure 3. Select examples of previously disclosed SERM/SERD AZD9496 **4** and CERAN/SERDs camizestrant **5**, giredestrant **6**, GDC-0927 **7**, imlunestrant **8**, and amcenestrant **9**.

clinical efficacy of these compounds, on-target toxicity remains a challenge. Hematologic and gastrointestinal toxicities complicate their use in combination with ET and may lead to tolerability issues due to drug−drug interaction (DDI).[26] Any new CERAN/SERDs in clinical development will be evaluated for their compatibility with CDK4/6 inhibitors.

As we began in 2014 to direct our medicinal chemistry program toward new ET drugs, we focused on addressing limitations of current drugs at the time: (1) incomplete ER antagonism of both WT and *mutESR1* (Tyr537Ser, Asp538Gly); and (2) suboptimal PK profile (i.e., poor oral bioavailability, short half-life, etc.).

We have recently described the details of key assays used for the identification of promising new ET.[6] The ovariectomized mouse uterine weight model is used to distinguish partial from complete ER antagonists by testing in both agonist mode (no E2) and antagonist mode (in the presence of E2) (Figure 4). Tamoxifen **1a** shows strong agonist activity and weak antagonist activity in this sensitive and informative model. By contrast, fulvestrant **3** compares to vehicle in both the agonist and antagonist modes. This result is characteristic of a CERAN in this model. To accelerate the evaluation of potential new antiestrogens, we sought an ex vivo model that would recapitulate the results of the in vivo uterine wet weight model. To achieve this objective, we employed an assay using cultured human uterine (Ishikawa) cells that have estrogen receptors and an AF1-responsive gene, alkaline phosphatase (AP), to assess ER functional activity (agonism/antagonism) by different ER ligands.[27] Compounds were incubated with Ishikawa cells for 72 h in the presence of E2 (antagonist mode) to measure ERα agonism (% E_{max}) through induction of alkaline phosphatase. CERANs are defined as those molecules that induce <15% E_{max} AP activity (agonist mode). Partial agonists exhibit 15−50% E_{max} activity, and full agonists show >50% E_{max} AP activity in the agonist format. In our studies,

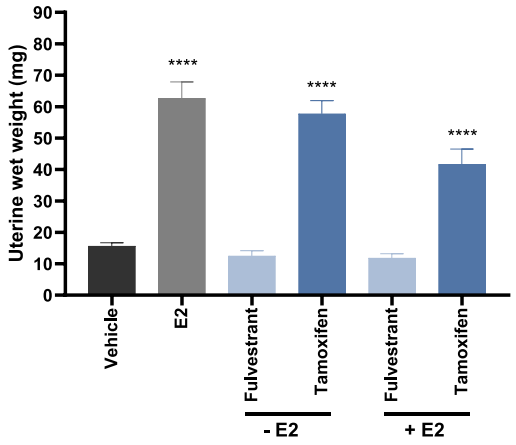

Figure 4. Fulvestrant **3** and tamoxifen **1a** tested in agonist (−E2) and antag. (+E2) modes in the ovariectomized mouse uterine weight model.[6] Adapted in part with permission from *Mol. Cancer Ther.* **2024**, *23* (3), 285−300. Copyright 2024, AACR Inc.

optimization of CERAN activity leads to complete receptor blockade and effective antitumor activity in ER+ breast cancer models.

While we monitored degradation of ER throughout the lead optimization effort, we view degradation as an epiphenomenon and not central to the drug optimization process, and viewed optimizing compound activity on ER degradation alone as insufficient.[6,14,28] Consistent with this view, Eikon has reported a poor correlation between ER degradation and efficacy, as assessed by cell proliferation in MCF7 and T47D cells.[29] To achieve robust tumor shrinkage, complete antagonism of any present ER is required.[14]

Using these tools, we initially identified benzopyran-based antagonists. Benzopyrans **10**[30] and **11**[31] (Figure 5) completely

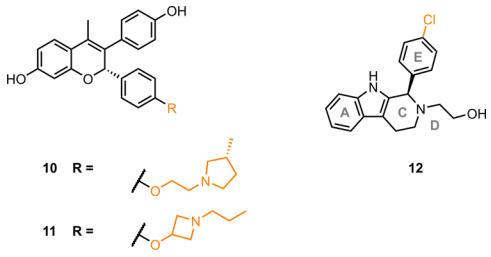

Figure 5. Benzopyrans **10** (pIC_{50} = 9.7 (AP, antag.)) and **11** (pIC_{50} = 10 (AP, antag.)) and tetrahydro-β-carboline ER hit **12** (pIC_{50} = 5.9 (binding)).

antagonized ER when tested in the AP assay (antag. mode). High-resolution X-ray cocrystal structures showed that the CERAN properties of benzopyran **10** can be attributed at least in part to the impact of the absolute configuration of the 3*R*-methyl of the pyrrolidine on the interaction of benzopyran **10** with ER.[30] This 3*R*-methyl interacts with helix 12 (H12), resulting in destabilization of the ER in this region. In contrast, the 3*S*-methyl does not disrupt H12. These data formed the basis of a structure-based hypothesis for the CERAN activity.

Compound **10** is a potent CERAN; however, we found that the PK properties of **10** did not justify further development.[30] Seragon has reported high clearance and low bioavailability of similar bis-phenol chromenes.[19] Although benzopyran **10** was ultimately abandoned as a lead molecule, the protein structural clues (H12 destabilization) provided by the cocrystal

https://doi.org/10.1021/acsomega.4c11023
ACS Omega 2025, 10, 22685−22700

structures of benzopyran **10** with the ER (PDB: 5UFX) guided further optimization, culminating in CERAN **21**.

We sought out a potent CERAN demonstrating complete WT and *mutESR1* blockade with a long half-life, leading to steady-state plateau levels with minimal peak-to-trough variability to support once daily oral dosing. To produce a CERAN with superior PK properties, we leveraged the ER binding hit, tetrahydro-β-carboline **12**, reported by AstraZeneca.[16] Tetrahydro-β-carboline **12** was unusual, as it does not contain a phenol mimicking similar functionality on the A-ring of E2. For E2, the A-ring phenol moiety contributes substantially to binding to the ER.[32] Indeed, a hydrogen bond between the tetrahydro-β-carboline NH and Leu346 of ERα replaces the key hydrogen bond made by the A-ring phenol of **10** with Glu353 and Arg394. Other groups have subsequently explored the tetrahydro-β-carboline scaffold as a starting point for developing CERAN/SERDs.[17,18,33−35]

RESULTS AND DISCUSSION

Based on our group's and others' work[16] at the time, we believed that the core heterocyclic structure of the carboline mimicked the interaction of E2 with ER and that the polycyclic core (Figures 5) would map onto the A-D rings of the steroid core (Figure 1 showing fulvestrant **3** with steroid A-D ring labels). Based on our experience, we hypothesized that the ER binding motif and the H12 interacting side chain, termed "E-ring," could be optimized to some extent independently. We remained, however, mindful of the observation that side chain SAR had been shown not to be fully portable from one ER binding motif to another.[36] We had previously shown[30] that R side chains containing basic amine functionality, such as pyrrolidine and azetidine, preferentially conferred superior antiestrogenicity through interaction with Asp351 and perturbation of H12 (Figure 6). Given that benzopyran **11** was a potent CERAN, we explored azetidine-containing side chains on the tetrahydro-β-carboline ER binding motif. We believed that this combination would permit optimization of CERAN and PK properties.[30]

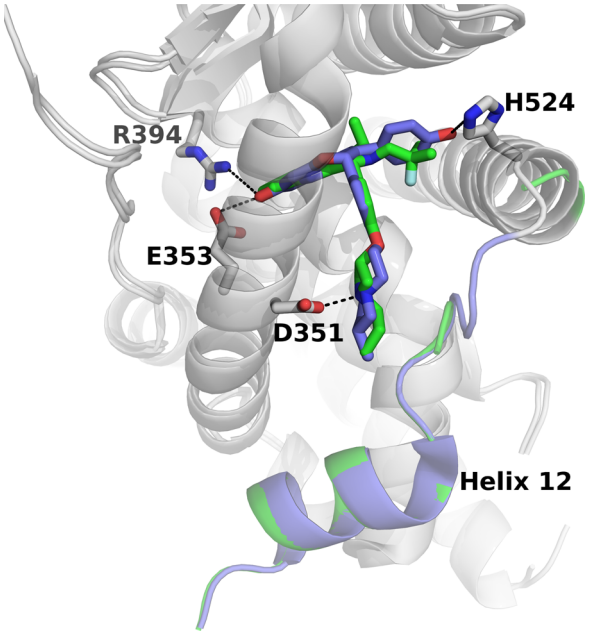

Figure 6. X-ray cocrystal structure of compound **21** (PDB: 8VV1) in green overlaid with **10** in blue.

Chemistry. Tetrahydro-β-carboline analogs were prepared from commercially available chiral Boc-protected tryptamine. After the removal of the Boc protecting group, tryptamine **16** was *N*-alkylated to introduce the D-ring mimic (DRM) (Scheme 1). Due to the steric hindrance around the alkyl DRM, a triflate is preferred as the leaving group. This substituted tryptamine was then condensed with substituted benzaldehydes under Pictet-Spengler conditions to afford the corresponding tetrahydro-β-carbolines. In the examples shown, the Pictet-Spengler reaction occurs with high *trans* diastereoselectivity (10:1 to >20:1). The major (1*R*, 3*R*) *trans* diastereoisomer is readily purified by chromatography. We established the *trans* stereochemistry by solving a small molecule X-ray structure of **21**-ACN solvate. We also confirmed the relative stereochemistry by preparing the (1*S*, 3*R*) cis isomer[37] (Supporting Information) and examining the proton NOE enhancements when the proton resonances on the chiral carbon centers are irradiated. The *trans* diastereoselectivity of the Pictet-Spengler reaction on N-substituted tryptamines has been previously studied.[38] The preparation of tetrahydro-β-carboline **21** is shown in Scheme 1. (See the Supporting Information for additional compound properties and characterization.)

Scheme 1. Synthesis of 21[a]

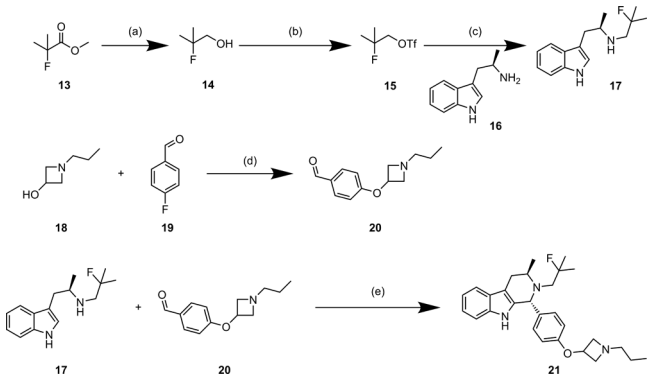

[a]Reagents and conditions: (a) $LiAlH_4$, diethyl ether, 0 °C, 63%; (b) Tf_2O, 2,6-lutidine, DCM, 0 °C, 86%; (c) DIEA, 1,4-dioxane, 90 °C, 32%; (d) Cs_2CO_3, DMF, 95 °C, 54% (e) AcOH, toluene, 80 °C, 22%.

Pharmacology. Previous SAR studies[36] on SERMs have shown that a three-atom linker between the phenyl E-ring and the basic amine (needed for interaction with Asp351) was preferred for antagonist activity. To test whether a 3-atom linker was suitable for CERAN activity in the context of the tetrahydro-β-carboline scaffold, analogs with tails D and E containing an *n*-propyl and an ethyleneoxy linker, respectively (Table 1) were prepared. Tails D and E have the azetidine distal to the E-ring. To assess the effect of rigidity in the 3-atom linker, compounds bearing tails F and G with the azetidine proximal to the E-ring were also evaluated. These combinations allowed for exploration of the relationship between the flexibility of the tail and functional activity. For tails E and G, oxygen was introduced in the linker to reduce possible oxidative metabolism at the benzylic position. Others also have reported exploration of Core C with Tail E and G.[35a]

Tail D on core A and C, as shown in analogs **22** and **29**, did not show antagonist activity and showed full agonist activity

https://doi.org/10.1021/acsomega.4c11023
ACS Omega 2025, 10, 22685−22700

Table 1. Data for Basic Side Chain Variation in the Ph, and 3-F-Ph, and 2,6-diF-Ph E-Ring Series[a]

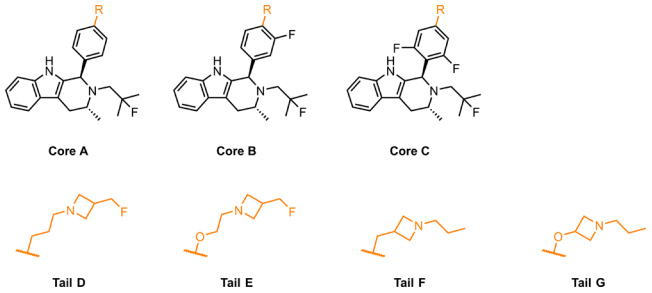

cpd	core	tail	ER binding pIC_{50}	AP (antag.) pIC_{50}	AP % E_{max}	cell prolif. pIC_{50}
fulvestrant **3**			9.0	8.5	0.1	7.9
21	A	G	8.7	8.5	0.3	7.7
22	A	D	8.8	NA	52	6.7
23	A	E	8.8	8.9	0.3	7.4
24	A	F	8.4	8.5	8.5	7.3
25	B	D	8.4	8.1	22	6.1
26	B	E	8.6	8.7	2.1	7.4
27	B	F	8.7	8.3	7.4	7.1
28	B	G	8.4	8.0	3.1	6.6
29	C	D	8.6	NA	79	7.3
30	C	E	8.6	9.1	0	7.6
31	C	F	8.3	8.8	5.4	7.5
32	C	G	8.7	8.8	0.3	7.4

[a]AP assays were run in Ishikawa cells in both antag. mode (+E2) and agonist mode. Cell proliferation assay was conducted in CAMA-1 WT cells. Arithmetic mean values are shown, 95% Confidence intervals (when $n \geq 3$) can be found in Tables S1−S3 of the Supporting Information.

with % E_{max} > 50 (Table 1). Analog **25**, which contains tail D on core B, showed partial agonist activity with an Emax of 22%. Tail D, among the 4 tail groups, confers the least antagonist activity. In contrast, tail F with the azetidine appended proximal to the E-ring shows improved antagonist activity but still retains low levels of agonist activity. The oxygen-containing tails E and G show no measurable agonism and the best antagonist activity across cores A, B, and C. Several analogs (**21**, **23**, **24**, **26**, **27**, and **29**−**32**) showed antiproliferative activity (pIC_{50} 7.1−7.7) in the CAMA-1 cell proliferation assay. CAMA-1 is an immortalized ER+, HER2- breast cancer cell line that expresses wildtype ESR1 and demonstrates transcriptional and maximal antiproliferative responses that align with the agonist/antagonist classifications determined using the AP assay.[6] We identified complete antagonists **21**, **23**, **30**, and **32** having the lowest % E_{max} (<1) when tested in AP agonist mode.

The length of the *N*-alkyl group of tail G-like compounds was briefly explored on Core A (Table 2). We found that the N-propyl chain length of tetrahydro-*β*-carboline **21** was optimal for full antagonist activity, whereas shorter or longer alkyl chain lengths led to a loss of antagonist activity. For example, analogue **35** with an *n*-butyl alkyl chain is a partial agonist. Further extension of the alkyl chain length to *n*-pentyl led to a full agonist, **36**. This steep functional activity cliff is difficult to rationalize by utilizing receptor docking models. A post hoc computational study using extended molecular dynamics simulations was conducted (see below for the discussion) to explain this observation.

A short study of DRM variation on Core L with Tail G was performed (Table 3). Compared to analogue **21**, analogs **38**, **40**, and **41** showed comparable or better antagonist activity in the AP assay. Removal of the hydrogen bond donor (HBD) of **38** by replacing OH with OMe led to a 1.5 log of potency loss

Table 2. Data for Core A; Tail G Alkyl Chain Length Variation

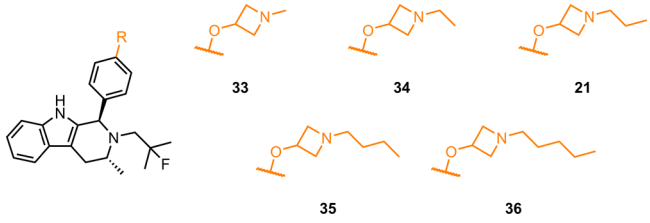

cpd	ER binding pIC_{50}	AP (antag.) pIC_{50}	AP % E_{max}
33	9.3	8.1	10
34	9.3	8.2	4.6
21	8.7	8.5	0.3
35	8.8	NA	27
36	8.6	NA	93

as seen in analog **41**. Modeling indicated that the hydroxyl of DRM N is within hydrogen bonding distance of His524. Steric bulk near the hydroxyl **39** led to a decrease in potency. In the CAMA-1 WT cell proliferation assay, analogue **21** exhibited better potency than analogs **38**, **40**, and **41**.

Antagonists **21**, **23**, **30**, and **32** were selected for further evaluation. These compounds exhibited good stability in mouse and human hepatocytes, showing half-lives >60 min (Table 4). The LipE of these compounds was in a range between 2.9 and 4.4. All of these compounds had shown low % E_{max} (<1; AP agonist mode). All four remained in contention and were advanced into in vivo evaluation (see in vivo assessment).

Structural Biology. Compound **21** Favors a unique ER*α* conformation compared to that of 4OHT **1b**.

To determine if compound **21**, when bound to ER*α*, would induce the receptor to adopt a conformation consistent with

https://doi.org/10.1021/acsomega.4c11023
ACS Omega 2025, 10, 22685−22700

Table 3. Data for D-Ring Mimic (DRM) Variation in the Ph E-Ring Series

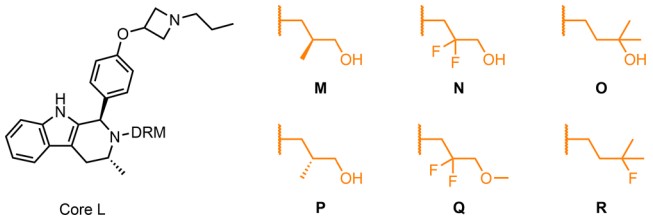

cpd	DRM[a]	ER binding pIC_{50}	AP[c] (antag.) pIC_{50}	AP % E_{max}	cell prolif. pIC_{50}
37	M	9.3	8.0	0.7	6.6
38	N	9.0	9.8	0	7.2
39	O	8.9	6.4	2.0	7.0
40	P	8.9	8.5	0.4	6.5
41	Q	9.0	8.3	0.9	6.5
42	R	7.8	7.3	0	<6

Table 4. Mouse and Human Hepatocyte Stability Data[a]

cpd	mouse hepatocyte Cl_{int} (μL/min/10^6 cells); half-life (min)	human hepatocyte Cl_{int} (μL/min/10^6 cells); half-life (min)	$cLogD_{7.4}$	LipE
21	<3.9; >360	10.7; 130	5.5	3.0
23	4.3; 322	6.1; 229	4.5	4.4
26	6.1; 227	5.1; 273	5.0	3.6
30	<3.9; >360	5.1; 270	5.0	4.1
31	<3.9; >360	<3.9; >360	5.2	3.5
32	<3.9; >360	4.3; 324	5.9	2.9
38	6.0; 230	18.2; 76	4.7	4.9
40	7.6; 183	8.8; 157	4.3	4.3
41	18.2; 76	14.1; 99	5.3	3.1

[a]LipE is calculated based on AP (antag.) pIC_{50}.

antagonism (similar to that seen for **10** (PDB: 5UFX)),[30] an X-ray cocrystal (2.0 Å) structure of compound **21** in complex with ERα ligand binding domain (LBD) was solved (PDB: 8VV1). Figure 6 shows a superposition of the **21** and **10**-bound ERα LBD cocrystal structures. A Cys381Ser/Cys417Ser/Cys530Ser/Leu536Ser mutant was used to facilitate crystallization while maintaining a WT-like antagonist conformation of H12.[16] Compound **21** does not have the polar interaction that compound **10** has with His524 (Figure 6). The interaction map (Figure 7, MOE) shows the expected hydrogen bond between the tetrahydro-β-carboline NH and Leu346 of ERα. The hydrogen bond between the protonated azetidine nitrogen and Asp351, commonly seen in cocrystal structures of antagonist-ER (PDB: 6ZOS;[16] PDB: 6WOK[33]), is also observed. Compound **21** is well-ordered in the orthosteric hormone binding pocket in each monomer of the

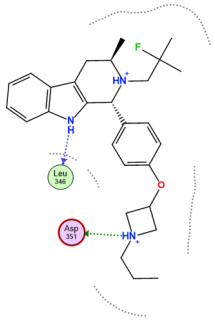

Figure 7. Interaction map showing Leu346 forming a hydrogen bond with indolic NH and Asp351 forming a hydrogen bond with the protonated azetidine of compound **21**.

canonical homodimer (Figure 8A). We were gratified to find that in this structure, helix 12 (H12) adopts the antagonist conformation by docking in the AF2 cleft via an LXXML motif.[39] This H12 orientation is homologous to that induced by other ER antagonists and is known to effectively block AF2 transcriptional coactivator binding in the AF2 cleft.[39,40]

The **21**-bound X-ray cocrystal structure also revealed what may be the molecular basis of its ER-degrading activities. Fulvestrant **3** destabilizes H12, exposing hydrophobic amino acids to solvent and inducing proteasomal degradation.[28a,41] SERDs, like **10**, exert similar effects on H12 but also increase the conformational mobility of the loop connecting helices 11 and 12 (H11−H12 loop).[30] Conversely, SERMs like 4-hydroxytamoxifen **1b** stabilize the H11−H12 loop and H12 and attenuate ER degradation.[44] The **21**-ER LBD X-ray cocrystal structure shows increased disorder of H12 and an overall poorly resolved loop connecting H11 to H12 (H11−H12 loop), as shown with increased b-factors, similar to the **10**-bound structure (Figure 8B).[30] In contrast, a SERM-like stabilization of this region is observed in the **1b**-bound X-ray cocrystal structure (Figure 8C).[5a]

It should be noted that crystal contacts were found near the H11−H12 loop and H12 in the B chain of the **21**/ERα LBD structure. All analysis is based solely on chain A. Likewise, the PDB: 5W9C model of 4-hydroxytamoxifen **1b** bound to ERα LBD was chosen because it is the same construct that was used for the **21**/ERα LBD cocrystal structure.[42] Together, these data show that compound **21** favors unique H11−H12 loop and H12 conformations compared to 4OHT **1b**.

*Compound **21** Differentially Impacts ER LBD Structural Features in Solution Compared to Fulvestrant (**3**).* Structural analysis of the **21**-ERα LBD complex suggested that it

https://doi.org/10.1021/acsomega.4c11023
ACS Omega 2025, 10, 22685−22700

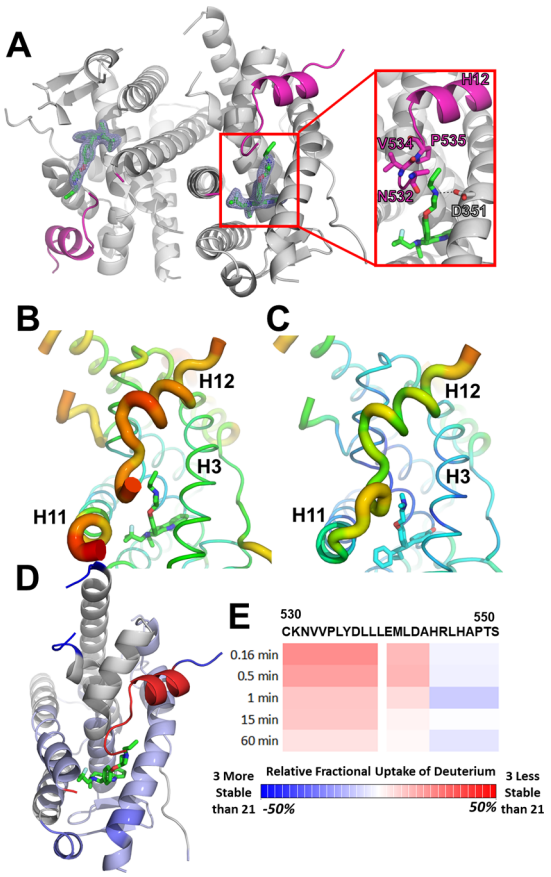

Figure 8. (a) X-ray cocrystal structure of compound **21** (green) in complex with ERα LBD. 2mFo-DFc map (blue mesh) contoured to 1.5 σ shows difference density in the absence of fit ligand. H11−H12 loop and H12 (magenta) are highlighted. (b) B-factor putty representation of the **21**-ERα LBD complex (PDB: 8VV1). (c) B-factor peptide representation of the 4-hydroxytamoxifen **1b**-ERα LBD complex (PDB: 5W9C). Cool (blue) colors and smaller diameter tubes indicate reduced B-factors, whereas hot (red) colors and larger diameter tubes indicate higher B-factors and increased conformational mobility. (d) Representation of HDX-MS data showing regions of ERα LBD with increased conformational mobility in the presence of compound **3** compared to compound **21**. (e) HDX-MS time-course heatmap for compound **3** versus compound **21** in the H11−H12 loop and H12. Hotter colors (red) indicate regions of relatively increased D_2O exchange or solvent accessibility, which are likely more conformationally mobile. Cooler colors (blues) indicate regions of less exchange that are more rigid.

mobilized the H11−H12 loop and H12. However, it was unclear as to whether it did so in a unique way compared to the aliphatic CERAN/SERD, fulvestrant **3**. As there is no published X-ray cocrystal structure of fulvestrant **3** in complex with ERα LBD, we used differential hydrogen−deuterium exchange mass spectrometry (HDX-MS) to understand how compound **21** affected ERα LBD dynamics in solution compared to unliganded (apo) and **3**-bound states. In HDX-MS, protein structural mobility correlates to a relative time-dependent exchange of deuterium (D_2O) with amide hydrogens. Highly dynamic regions will exchange more deuterium over time relative to rigid regions.[43] The profile of fulvestrant **3** agrees with an earlier HDX-MS study.[5a,44] Overall, CERAN/SERDs **21** and **3** show similar HDX-MS profiles when compared with unliganded (apo) LBD (Figure S3). Direct comparison of **3** to tetrahydro-β-carboline **21** shows significant dynamic differences in the H11−H12 loop and H12 region (residues 530−550). The H11−H12 loop and most H12 are less stable (more dynamic) in the presence of fulvestrant **3** compared to tetrahydro-β-carboline **21** at early time points. Eventually, these differences become less apparent. Conversely, the C-terminal end of helix 12 appears to be more stable in solution when compound **21** is bound to ER LBD compared to fulvestrant **3** (Figure 6E).

In the absence of an experimental structure of the **3**-ER LBD complex, we can only speculate that its long aliphatic side arm directly perturbs residues near the N-terminus of H12, including Leu536, Tyr537, and Asp538, to mobilize this region. While more time is required for fulvestrant **3** to exert the same effects on this region. At the same time, compound **21** can access spaces within the hormone binding pocket that are likely sterically precluded for the long side arm of fulvestrant **3**, allowing for H12 structural perturbations near the c-terminus. Together, these data show that compound **21** and fulvestrant **3** favor distinctive ERα conformational ensembles in solution, and further studies are needed to mechanistically define how these different structures impact ER biology.

Molecular Dynamics Simulations. *Interplay of Ligand Energetics, Dynamics, and Protein Fluctuations Drive CERAN Activities.* Our X-ray cocrystal structural analysis suggested that the *n*-propyl group of tetrahydro-β-carboline **21** near the H11−H12 loop and H12 likely adopted multiple torsion angle geometries. Further, HDX-MS showed a D_2O uptake profile indicating that tetrahydro-β-carboline **21** differentially affects the dynamics of this LBD region in solution compared to fulvestrant **3**. To better understand the structural basis of CERAN activities, we performed atomistic molecular dynamics simulations of tetrahydro-β-carboline **21**, alongside analogous compounds with terminal alkyl chain lengths between *n*-ethyl **34**, *n*-butyl **35**, and *n*-pentyl **36**. Across the simulations, interaction analysis shows that, as suggested in the crystal structure, the *n*-propylazetidine of tetrahydro-β-carboline **21** adopts a significantly different pose between the start and the end of the simulation (Supporting Information Figure S6A). Whereby, it is initially positioned near H3, then reorients to form a hydrogen bond with Asp351 and interacts with Pro535. In doing so, a water molecule can now infiltrate and sample a hydrogen bond with the azetidine group. During the simulation, Phe404 picks up a π-π interaction with the benzo-ring of **21**'s core, further stabilizing the complex, unlike compounds **34**, **35**, and **36**. Interaction analysis also shows that the *n*-propyl group is the ideal carbon length to interact with H12. Ethylazetidine of tetrahydro-β-carboline **34** stays docked near H3 throughout the simulation and is not predicted to affect H12 in the same way that would favor the antagonist conformation of the receptor (Supporting Information Figure S6B). Increasing the length to *n*-butyl **35** and *n*-pentyl **36** groups favors the H11−H12 loop and H12 facing orientation throughout the simulation, but no new interactions are observed with the extra carbons heading out toward solvent (Supporting Information Figure S6C/D). Therefore, these ligands are less efficient than the *n*-propyl group at inducing the therapeutically critical receptor conformation. In this case, where receptor docking was not helpful, MD simulations showed a preference for the *n*-propylazetidine of tetrahydro-β-carboline **21**.

In Vivo Assessment. Mouse pharmacokinetic data for compounds **21**, **23**, **30**, and **32** are summarized in Table 5.

https://doi.org/10.1021/acsomega.4c11023
ACS Omega 2025, 10, 22685−22700

Compounds **21** and **32** had the highest total drug exposure and the longest half-lives among these compounds.

Table 5. In Vivo Mouse Oral Single Dose PK Data for Compounds 21, 23, 30, and 32

	mouse PK				
cpd	C_{max} (ng/mL)	$t_{1/2}$ (h)	total AUC_{inf} (h·ng/mL)	% free drug in plasma	free AUC_{inf} (h·ng/mL)
21	121	18	2477	0.06	1.5
23	186	7	2289	0.17	3.9
30	112	11	2090	0.04	0.8
32	219	15	2743	0.01	0.3

However, compound **32** had the lowest free fraction and the lowest free drug exposure. Total plasma drug concentrations of all four compounds over 24 h (sparse blood sampling at 1, 4, 8, and 24 h) are depicted in Figure 9. As compounds **21** and **23** had relatively higher free plasma exposures (free AUC_{inf}, estimated based on the percent free fraction), they were advanced to the mouse uterine wet weight and xenograft studies.

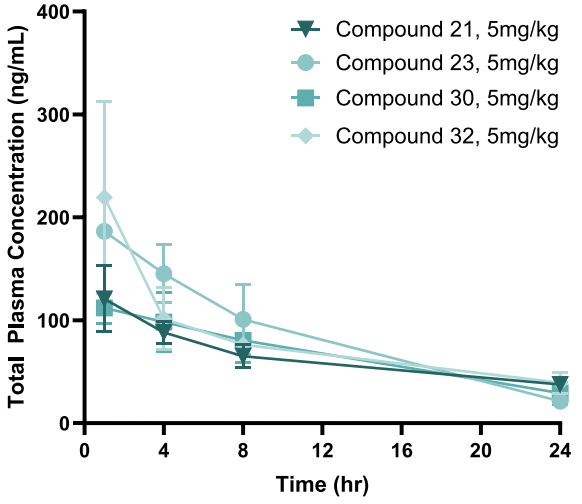

Figure 9. Total drug concentrations in mouse for compounds **21**, **23**, **30**, and **32** from single dose oral PK studies.

In the uterine wet weight studies, compounds **21** and **23** were evaluated for their ability to inhibit an E2-induced increase in uterine wet weight (Figure 10). Both compounds inhibited uterine wet weight gain in a dose-dependent manner. A comparable E2-induced inhibition comparable to that of fulvestrant **3** was observed at or above 1 mg/kg doses of compounds **21** and **23**. Doses that resulted in 50% inhibition of E2-induced uterine wet weight (ID_{50}) are presented in Table 6. Compound **21** was more potent than compound **23** in this assay.

Characterization of compounds **21**, **23**, **30**, and **32** indicated that they displayed comparable antiproliferative effects in MCF7 cells (Table S4). In an ER+ breast cancer (MCF7) mouse xenograft model, compounds **21** and **23** were evaluated for the ability to inhibit tumor growth at oral doses of 10 mg/kg/day for 36 days (Figure 11a). This dose was chosen based on anticipated pharmacokinetics to be within the efficacious range.

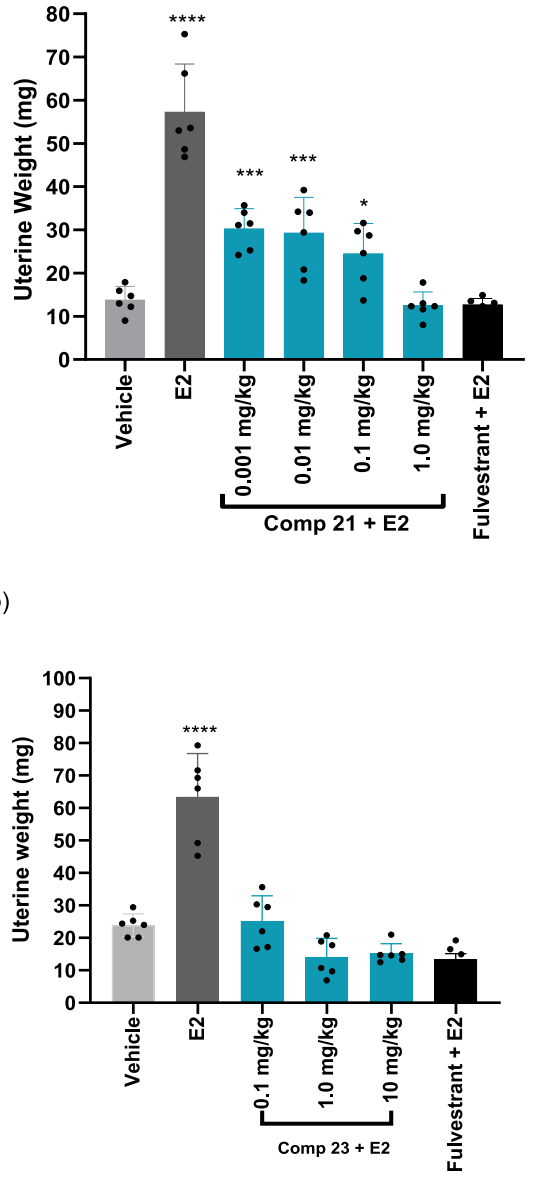

Figure 10. Mouse uterine weight data for compounds (a) **21** and (b) **23** (statistically significant differences from vehicle group is denoted by asterisks; *$p < 0.05$; **$p < 0.01$, ***$p < 0.001$).

Table 6. Mouse Uterine Weight Data for Compounds 21 and 23

cpd	uterine wet weight ID_{50} (mg/kg)
21	<0.001
23	<0.1

Both compounds caused complete tumor growth inhibition (TGI), but compound **21** showed a qualitatively better response across the entire group, with the least mean tumor volume at the end of the study on day 36 (Figure 11b). Vehicle group animals were euthanized on day 22, and the individual tumor volumes on that day across all groups were presented in Figure 11b. Similar to the results of the uterine wet weight study, compound **21** was better than compound **23** in the xenograft study. As a result, compound **21** was advanced to further development.

In a reporter assay of gene transcription activity, compound **21** inhibited both ERα- and ERβ-mediated gene activity with

https://doi.org/10.1021/acsomega.4c11023
ACS Omega 2025, 10, 22685−22700

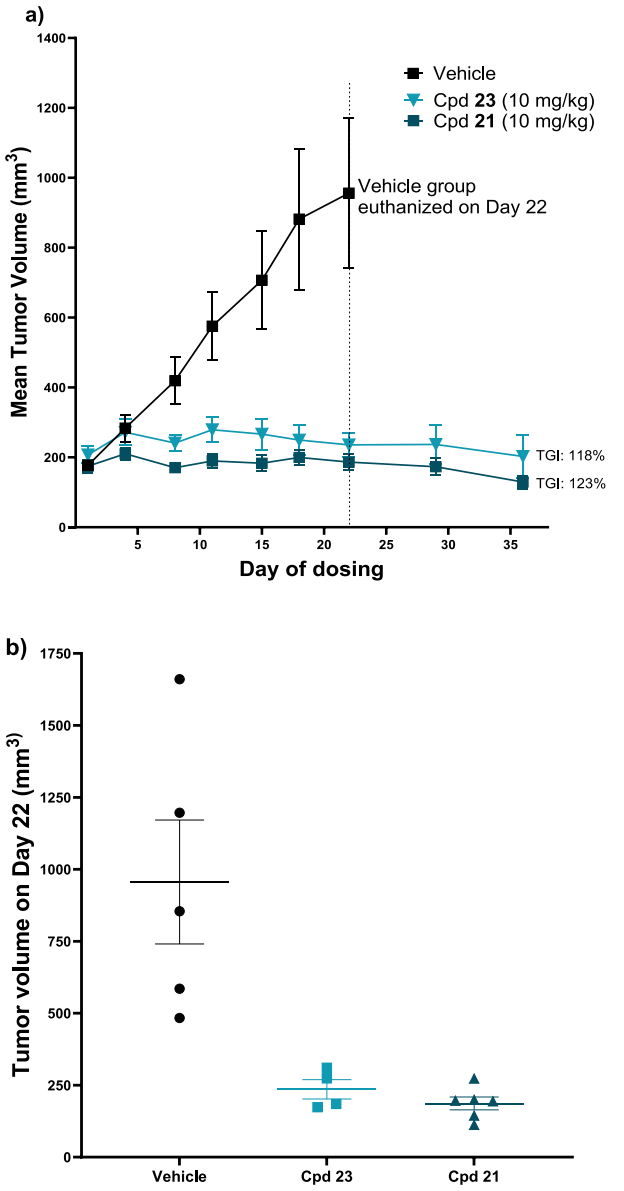

Figure 11. (a) Change in tumor volume over time after daily oral dosing with **21** and **23** at 10 mg/kg in MCF-7 tumor model; (b) tumor volume (mm^3) on Day 22 after daily oral dosing with **21** and **23** at 10 mg/kg in the MCF-7 tumor model.

pIC_{50} values of 9.0 and 8.5, respectively (Table 7). Compound **21** demonstrated no agonist cross-reactivity on GR, PR, or AR. However, compound **21** did inhibit agonist-induced activity of AR in a reporter assay with a pIC_{50} of 5.8.

Compound **21** was profiled in vitro using Ishikawa and CAMA-1 cells engineered to express Asp538Gly or Tyr537Ser mutant ER, as well as the patient-derived line, ST941/C,[45] which heterozygously expresses *ESR1*^{Tyr537Ser}. In all assays, compound **21** demonstrated antagonist activity, however, potency was reduced in cells harboring the activating mutations, Asp538Gly and Tyr537Ser, compared to WT (Table 8). Compound **21** was also found to be an effective degrader of ERα (Figure 12a–c). In both WT and *ESR1*^{Tyr537Ser} mutant cell lines and compound **21** demonstrated comparable degradation activity to imlunestrant **8**. In the *ESR1*^{Asp538Gly} mutant cell line, the degradation activity of compound **21** was comparable to camizestrant **5** and giredestrant **6**. In the MCF-7 cell line, the degradation activity of compound **21** and fulvestrant **3** was also comparable (Figure 12d).

Table 7. Nuclear Hormone Receptor Off-Target activity for 21

	ERα	Erβ	GR	PR	AR
mode	pIC_{50}	pIC_{50}	pIC_{50}	pIC_{50}	pIC_{50}
agonist mode	<5.5	<5.5	<5.5	<5.5	<5.5
antag. mode	9.0	8.5	<5.5	<5.5	5.8

Table 8. In Vitro Mutant *ESR1* Cell Activity of Compound 21

	AP (antag.)	CAMA-1 cell prolif.	ST941/C cell prolif.
	pIC_{50}	pIC_{50}	pIC_{50}
ESR1^{WT}	8.6	8.8	NA
ESR1^{Asp538Gly}	7.5	8.2	NA
ESR1^{Tyr537Ser}	7.3	7.9	7.5

Compound **21** is highly plasma protein-bound (>99%) across all species, including humans. Plasma free drug percentages in mouse/rat/dog/cyno/hu are 0.06/0.24/0.04/0.13/0.08, respectively. The human unbound fraction of compound **21** is highly comparable in both nonclinical efficacy evaluation species (mouse) and toxicity evaluation species (rats and dogs). All nonclinical efficacy and safety evaluations are likely to be pertinent to the clinical efficacy and safety. Low risk of transporter inhibition by compound **21** was determined by in vitro P-gp and BCRP assays (IC_{50} = 4 and >5 μM, respectively). No inhibitory activity was observed for the CYP 3A4 isoform (IC_{50} > 10 μM). Based on these data, no clinically relevant drug–drug interaction liability is anticipated against substrates of these enzymes. Compound **21** did not inhibit the human ether a-go-go related gene (hERG) protein at 30 μM and hence does not carry cardiac arrhythmia liability.

Compound **21** is orally bioavailable and has low clearance and a long half-life in the mouse, rat, dog, and monkey (Table 9). The half-lives after a single oral dose in the mouse, rat, dog, and monkey were 10, 16, 106, and 34 h, respectively. The in vivo clearance in mice was found to be in good agreement with that predicted from the in vitro hepatocyte data.

In ST941/C, an *ESR1*^{Tyr537Ser} patient derived xenograft model, a dose-dependent increase in tumor growth inhibition and regression was observed (Figure 13), Compound **21** at 3 and 10 mg/kg doses were superior to fulvestrant **3** in this model.

CONCLUSIONS

Exploration of tetrahydro-β-carboline as a steroidal core mimic, followed by optimization of the E-ring for complete antagonist activity, led to the discovery of tetrahydro-β-carboline **21**. Complete antagonism was confirmed by the lack of ER agonism observed in the AP assay and the immature ovariectomized mouse uterus model. Furthermore, tetrahydro-β-carboline **21** demonstrated robust antitumor efficacy in both MCF-7 and ST941/C mouse xenograft tumor models. Overall, these data supported the advancement of palazestrant (**21**, **OP-1250**) as a new investigational drug in the oral CERAN/SERD class. Structural biology studies confirmed the binding of **21** in ERα and the resulting movement of H12, consistent

https://doi.org/10.1021/acsomega.4c11023
ACS Omega 2025, 10, 22685−22700

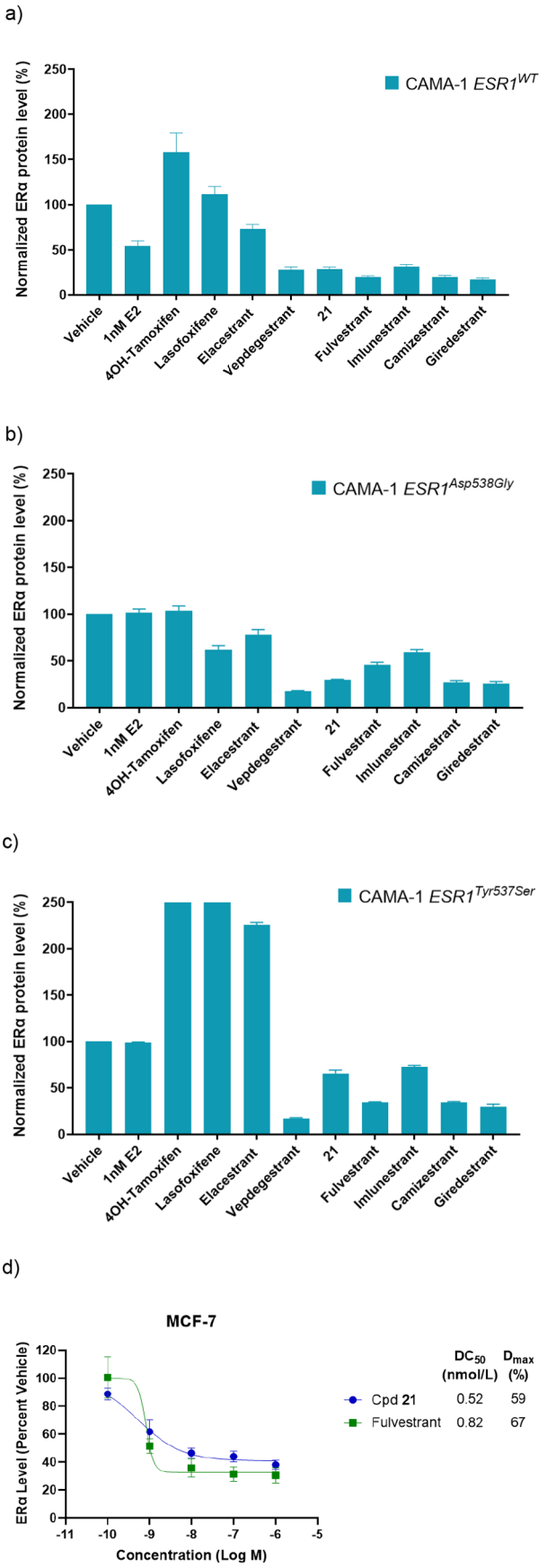

Figure 12. ERα protein levels following 24 h treatment with 316 nM of compound **21**, and competitor molecules in (a) CAMA-1 $ESR1^{WT}$, (b) CAMA-1 $ESR1^{Asp538Gly}$, (c) CAMA-1 $ESR1^{Tyr537Ser}$, and (d) ERα protein levels following 24 h treatment with dose response of compound **21** and fulvestrant **3** in MCF-7 cells.

with an antagonist receptor conformation. Palazestrant (**21**) is currently being evaluated in a phase 3 clinical trial in patients with advanced ER-positive breast cancer.

EXPERIMENTAL SECTION

Chemistry. Unless otherwise stated, all chemicals were purchased from commercial suppliers and used without further purification. Thin-layer chromatography (TLC) was performed using glass-backed silica-coated plates. TLC plates were visualized under ultraviolet light and/or with stains (potassium permanganate, phosphomolybdic acid, p-anisaldehyde). The ^{1}H NMRs were recorded on Bruker Avance III HD 400/Bruker Avance III HD 500/Bruker Avance NEO 400/Bruker Avance NEO 500, [^{1}H (400 MHz/500 MHz), ^{13}C (100 MHz/125 MHz)] with complete proton decoupling for ^{13}C. Chemical shifts were analyzed on Topspin software. Chemical shifts are reported in parts per million with the solvent resonance as the internal standard ($CDCl_3$, ^{1}H: δ 7.26 ppm, ^{13}C: δ 76.99 ppm). Coupling constants are reported in Hertz (Hz). Abbreviations are used as follows: s = singlet, d = doublet, t = triplet, q = quartet, hept = heptet, m = multiplet, and dd = doublet of doublet. Samples were analyzed on an LC−MS with Waters Acquity UPLC-MS (Acquity UPLC BEH C18 50 mm × 2.1 mm or YMC Trait C18, 30 mm × 2.1 mm) mass spectrometer (electrospray ionization) liquid chromatograph system. Waters e-2965 HPLC-MS (X-bridge C18, 100 mm × 4.6 mm) mass spectrometer (electrospray ionization) liquid chromatograph system equipped with 2998PDA detector and Agilent1260-II ELSD detector. HPLC was analyzed with a Waters Acquity UPLC (Acquity UPLC BEH C18 100 × 2.1 mm or an X-bridge C18 150 × 4.6 mm) liquid chromatograph system with a 2998 PDA detector. Optical rotation of chiral materials was analyzed with a JASCO P-2000 Polarimeter. HRMS samples were analyzed with a Thermo Scientific Orbitrap Exploris 240 mass spectrometer (Electrospray ionization- ESI), a liquid chromatograph system. VCD samples were analyzed by the FVS-6000 instrument using the MCT_V detector. Chiral SFC samples were analyzed with Waters Acquity UPC2; chiral column: (*R*,*R*) WHELK-01 (4.6 × 150) mm, 3.5 μm, with liquid carbon dioxide and 0.5% diethylamine in methanol as eluent, equipped with 2998PDA detector.

All compounds are >95% pure by HPLC.

2-Fluoro-2-methylpropanol ***14.*** $LiAlH_4$ (176 mL, 1 M in THF) was added to anhydrous diethyl ether (300 mL) at 0 °C. Methyl 2-fluoro-2-methylpropionate (14.6 g, 118.0 mmol) was added dropwise over 1 h. The suspension was stirred for 1.5 h. Ten milliliters of water were added dropwise, followed by 10 mL of 2 M NaOH and another 10 mL of water. The quenched reaction mixture was stirred overnight (heated to rt). The white suspension was filtered, and the filter cake was washed with CH_2Cl_2. The filtrate was concentrated to give the title product (7.2 g, 63% yield). ^{1}H NMR ($CDCl_3$, 300 MHz): δ 3.56 (dd, 2H, J = 20.4, 6.3 Hz), 1.85 (t, 1H, J = 6.2 Hz), 1.40 (s, 3H), 1.33 (s, 3H).

2-Fluoro-2-methylpropyl Trifluoromethanesulfonate ***15.*** Trifluoromethanesulfonic anhydride (5.0 mL, 29.7 mmol) was

https://doi.org/10.1021/acsomega.4c11023
ACS Omega 2025, 10, 22685−22700

Table 9. Single-Dose Pharmacokinetics of Compound 21 in the Mouse, Rat, Dog, and Monkey

species	mouse		rat		dog		monkey	
route	PO	IV	PO	IV	PO	IV	PO	IV
dose (mg/kg)	5	0.5	5	0.5	10	10	10	3
C_{max} (ng/mL)	91	29	138	313	1760	4060	170	651
T_{max} (h)	1	NA	1.5	NA	1.5	NA	8	NA
AUC (ng·h/mL)	1030	161	2590	454	33700	41300	5090	3420
V_d (L/kg)	NA	27	NA	8	NA	16	NA	49
CL (L/h/kg)	NA	3.1	NA	0.8	NA	0.2	NA	0.8
$T_{1/2}$ (h)	10	7	16	7	106	63	34	42
F (%)	72	NA	55	NA	89	NA	44.4	NA

added dropwise to a 0 °C solution of 2-fluoro-2-methylpropanol (2.1 g, 22.7 mmol) and 2,6-lutidine (3.4 mL, 29.4 mmol) in CH_2Cl_2 (25 mL) over 30 min. After 2 h, the solution changed from red to light brown. TLC indicated that the starting material was not present. The reaction mixture was washed with 1 M HCl (2 × 20 mL) and saturated aqueous sodium bicarbonate solution (2 × 20 mL), and the aqueous layers were each back-extracted with CH_2Cl_2 (20 mL). The combined organic layers were dried over sodium sulfate, and the solution was concentrated under reduced pressure to yield the title product (4.39 g, 86% yield). ^{1}H NMR ($CDCl_3$, 300 MHz): δ 4.41 (d, 2H, J = 18.6 Hz), 1.46 (d, 6H, J = 20.4 Hz), ^{19}F NMR ($CDCl_3$, 282 MHz): δ −147.1, −74.5.

(R)-N-(1-(1H-indol-3-yl)propan-2-yl)-2-fluoro-2-methylpropan-1-amine ***17***. 2-Fluoro-2-methylpropyl trifluoromethanesulfonate (2.5 g, 11.0 mmol) was added to an anhydrous solution of (2*R*)-1-(1*H*-indol-3-yl)propan-2-amine (1.2 g, 6.9 mmol) and DIEA (1.1 g, 8.4 mmol) in 1,4-dioxane (30 mL), and the mixture was heated to 90 °C for 16 h. EtOAc (40 mL) was added, and the solution was washed with saturated aqueous sodium bicarbonate solution (2 × 20 mL). The combined aqueous layers were back-extracted with EtOAc (2 × 20 mL), and the combined organic layers were dried over sodium sulfate, filtered, and dried in vacuo. The crude product was purified via flash silica gel chromatography in 0−10% MeOH in DCM to give the title product (550 mg, 32% yield). ^{1}H NMR ($CDCl_3$, 300 MHz): δ 8.18 (br s, 1H), 7.64 (d, 1H), 7.36 (d, 1H), 7.26−7.11 (m, 2H), 7.03 (d, 1H), 3.05 (m 1H), 2.95−2.68 (m, 4H), 1.37 (dd, 6H, J = 21.9 Hz), 1.13 (d, 3H). ^{19}F NMR ($CDCl_3$, 282 MHz): δ −144.2.

4-((1-Propylazetidin-3-yl)oxy)benzaldehyde ***20***. 4-Fluorobenzaldehyde (2.8 mL, 25.3 mmol), 1-propylazetidin-3-ol (3.2 g, 27.8 mmol), cesium carbonate (17.2 g, 52.8 mmol), and DMF (60 mL) were stirred under argon at 95 °C for 6 h and allowed to cool to room temperature. The solid was removed under filtration, and the filtrate was concentrated. The resulting residue was diluted with EtOAc (100 mL) and water (80 mL). The organic layer was washed with brine (5 × 50 mL), dried over sodium sulfate, filtered, and dried in vacuo. The crude product was purified via flash silica gel chromatography in 0−50% EtOAc in hexanes to give the title product (3.0 g, 54% yield). ^{1}H NMR ($CDCl_3$, 300 MHz): δ 9.88 (s, 1H), 7.81 (d, 2H, J = 8.7 Hz), 6.87 (d, 2H, J = 8.1 Hz), 4.89−4.85 (m, 1H), 3.83 (t, 2H, J = 6.0 Hz), 3.11 (t, 2H, J = 7.4 Hz), 2.48 (t, 2H, J = 7.5 Hz), 1.44−1.37 (m, 2H), 0.91 (t, 3H, J = 7.2 Hz).

(1R,3R)-2-(2-Fluoro-2-methylpropyl)-3-methyl-1-(4-((1-propylazetidin-3-yl)oxy)phenyl)-2,3,4,9-tetrahydro-1H-pyrido[3,4-b]indole ***21***. 4-((1-Propylazetidin-3-yl)oxy)-benzaldehyde (124 mg, 0.6 mmol) was added to a solution of (*R*)-N-(1-(1*H*-indol-3-yl)propan-2-yl)-2-fluoro-2-methylpropan-1-amine (100 mg, 0.4 mmol), glacial acetic acid (0.50 mL, 8.7 mmol), and dry toluene (5.0 mL, 47.2 mmol) over 4 Å molecular sieves. The solution was stirred at 80 °C for 10 h. The reaction was allowed to cool to room temperature and diluted with CH_2Cl_2, washed with saturated aqueous sodium bicarbonate solution, dried over sodium sulfate, and dried in vacuo. The crude was purified via reverse-phase HPLC (Kinetex 5 μm C18 100 Å column; size: 100 mm × 30.0 mm; 40−90% ACN in water) to give the title product as a white solid (39 mg, 22% yield). ^{1}H NMR (400 MHz, $CDCl_3$): δ 8.00 (brs, 1H), 7.52 (d, J = 7.2 Hz, 1H), 7.26−7.24 (m, 1H), 7.17 (d, J = 8.4 Hz, 1H), 7.14−7.08 (m, 3H), 6.64 (dd, J = 2.8 Hz, 11.2 Hz, 2H), 5.00 (brs, 1H), 4.62 (quin, J = 5.6 Hz, 1H), 3.79−3.73 (m, 2H), 3.33 (brs, 1H), 3.02 (t, J = 6.8 Hz, 2H), 2.75−2.45 (m, 4H), 2.44−2.42 (m, 2H), 1.44 (d, J = 21.6 Hz, 3H), 1.39−1.33 (m, 2H), 1.28 (d, J = 21.6 Hz, 3H), 1.07 (d, J = 6.8 Hz, 3H), 0.89 (t, J = 7.2 Hz, 3H). ^{13}C NMR (100 MHz, $CDCl_3$): 156.4, 136.4, 135.1, 133.4, 130.4, 127.4, 121.5, 119.2, 118.1, 114.1, 110.8, 110.1, 97.9 (d, J = 165.1 Hz), 66.6, 62.0, 61.6, 61.5, 54.3, 47.6, 25.7 (d, J = 23.2 Hz), 25.01 (d, J = 24.8 Hz), 21.0, 11.8. ^{19}F NMR (376 MHz, $CDCl_3$): −140.30. HRMS (ESI): $C_{28}H_{37}FN_3O$ $[M + H]^+$ calcd 450.2916, found: 450.2915. HPLC: 99.23%. Chiral purity = 99.8% de; 99.8% ee. $[\alpha]^{20}$D: −4 (c 0.1, acetonitrile).

Reagents, Cells, and In Vitro Studies. CAMA-1 and Ishikawa (originally ECC-1) cell lines were purchased from ATCC (Manassas, VA, USA). The ST941C cell line was obtained under a license from XenoSTART (San Antonio, TX, USA). Cell lines were authenticated using short tandem repeat (STR) DNA profiling and tested for mycoplasma at Laragen (Culver City, CA, USA). Cells were cultured for no more than 30 passages following reanimation. Cell lines were cultured in medium containing 10% fetal bovine serum (FBS) (#SH30070.03, Cytiva; Marlborough, MA, USA) or medium supplemented with the listed concentration of charcoal/dextran stripped (CDS) FBS (#SH30068.03, Cytiva). Media used were Richter's IMEM (#A1048801 Gibco) supplemented with nonessential amino acids (Gibco #11140-050) for CAMA-1, RPMI 1640 (#A104910 Gibco) supplemented with 10 mM HEPES (#15630-080 Gibco) and 1 mM sodium pyruvate (#11360-070 Gibco) for Ishikawa, and RPMI 1640 (#A1049101 Gibco) for ST941C. All cell lines were additionally supplemented with 1% GlutaMax (#35050061 ThermoFisher Scientific; Waltham, MA, USA). E2 (no. E8875) and fulvestrant (no. I4409) were purchased from Millipore Sigma (Burlington, MA, USA).

ERα ligand binding was assayed using the LanthaScreen time-resolved fluorescence energy transfer (TR-FRET) ERα competitive binding assay (no. A15887 ThermoFisher

https://doi.org/10.1021/acsomega.4c11023
ACS Omega 2025, 10, 22685−22700

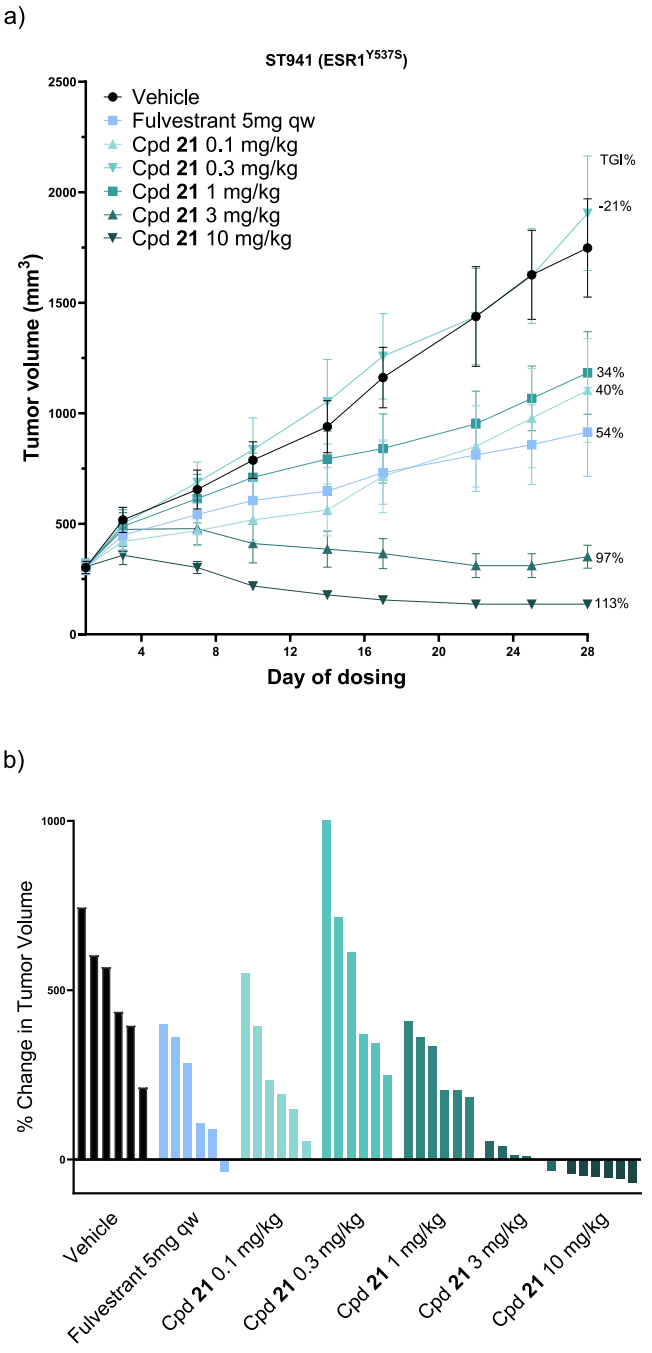

Figure 13. (a) Change in the tumor volume over time with different doses of **21** in ST941/C (*ESR1*^{Tyr537Ser}) tumor model; (b) waterfall plot of percent change in the tumor volume of individual animals within each group.

Scientific), per manufacturer's protocol. Following 2-h incubation at room temperature, compound binding was measured as a decrease in TR-FRET and normalized to 10 μM E2 and dimethyl sulfoxide (DMSO) vehicle.

For the AP assay, Ishikawa cells were plated in medium containing 4.8% charcoal/dextran stripped (CDS) FBS. At least 4 h later, cells were treated with compounds in the same volume of media without CDS FBS. Cells were incubated for 3 days, the medium was removed, and the plates were frozen at −80 °C. Thawed plates were incubated with a chromogenic substrate of AP, *p*-nitrophenyl phosphate (#02212 Thermo-Fisher Scientific), for 90 min at 37 °C, and absorbance was read at 405 nm. For antagonist mode assays, cells were cotreated with 500 pM E2.

Cellular proliferation of breast cancer cells was measured using CyQUANT, a fluorescent DNA-binding dye (#C7026 Invitrogen; Waltham, MA, USA). Cells were treated with compounds in duplicate in medium containing 4.8% CDS FBS in the presence of 100 pM E2 unless otherwise noted. Treated plates were incubated for 7 days prior to harvest. Following incubation, the medium was removed and the plates were frozen at −80 °C. Thawed plates were prepared and quantified per the manufacturer's protocol. Fluorescent activity was normalized to the activity of E2 alone, and replicates with values >130% of E2 vehicle were excluded from analysis.

Data for LanthaScreen, AP, and cellular proliferation assays were normalized to the E2 vehicle control for each assay and expressed as percent total response. IC_{50} or EC_{50} values were calculated in Prism software using a four-parameter fit. Emax is the percent effect at the highest drug concentration for each treatment, where 100% represents maximal response and 0% is no change from vehicle control.

To determine free fraction, plasma protein binding experiments were conducted in a 48-well plate using a rapid equilibrium dialysis format. One μM of test compounds was incubated in undiluted plasma from humans, rats, mice, dogs, and monkeys for 4 h at 37 °C to determine the percent unbound drug using LC−MS/MS.

To evaluate the test compound **21** as a P-gp and BCRP inhibitor, the solvent control, test compound, or inhibitors in DMSO were added to the membrane vesicles (1% v/v of the final reaction volume) and were preincubated for 15 min at 37 ± 2 °C. After preincubation, the incubation was initiated by the addition of the probe substrate and MgATP (4 mM) or MgAMP (4 mM) in incubation medium and incubated for the designated time. At the end of the incubation period, an aliquot was collected for recovery measurement by LC−MS/MS.

To evaluate the test compound **21** as an inhibitor of CYP enzymes, the test compound was incubated with probe substrate and human liver microsomes at approximately 37 ± 2 °C in a buffer mixture (described in the table below) in accordance with SOPL3250.13 or 0.14. Due to the possibility that the test article may bind to microsomal protein or lipids, experiments were performed using a low microsomal protein concentration and short incubation time (5 min). Reactions were initiated by the addition of cofactor and were terminated by the addition of the appropriate stop reagent containing internal standard (deuterated probe substrate metabolite). The stop reagent was acetonitrile. The samples were centrifuged at 920 × *g* for 10 min at 10 °C, and the supernatant fractions were analyzed by LC−MS/MS.

The hERG patch clamp assay uses ionic currents to determine the inhibition potential of compound **21** in hERG ion channels. Compound **21**'s inhibition of hERG was tested at concentrations ranging from 3 to 100 μM.

Animal Studies. Uterine wet weight studies were performed using ovariectomized BALB/c mice (7−8 weeks old), which were purchased from Charles River Laboratories. Studies were conducted at Bayside BioSciences in accordance with established protocol approved by the vendor's Institutional Animal Care and Use Committees (IACUC). On the seventh day after ovariectomy, mice were administered vehicle or E2 at 0.1 mg/mouse subcutaneously in combination with vehicle or antiestrogenic compounds, orally, once daily, for 3

https://doi.org/10.1021/acsomega.4c11023
ACS Omega 2025, 10, 22685−22700

days. The mice were euthanized 24 h after the last dose, and uterine samples were harvested and weighed. Fulvestrant **3** was administered at 5 mg/dose subcutaneously.

Pharmacokinetic studies were performed using BALB/c mice, athymic nude mice, Sprague−Dawley rats, or Beagle dogs that were administered the test article orally either as a single dose or repeat dose, and the pharmacokinetic profile over a 24 h period was measured on day 1 and at steady state (28 days). The test article formulation used in pharmacokinetic studies was 0.5% CMC in 1xPBS.

Xenograft studies were performed using female, immunodeficient athymic nude mice (Taconic or Jackson) that were supplemented with estradiol and implanted with an ER+ breast cancer cell line, MCF7 or patient-derived XenoSTART cell line ST941, subcutaneously in the mammary fat region. These animals were randomized into groups when the tumor volume reached ∼150 mm^3. Mice were treated daily with either the vehicle or the test article. The vehicle and test article formulation used in both uterine wet weight and xenograft studies was 2.5% DMSO, 97.5% of 0.5% CMC-Na suspension. Tumor volume and body weights were recorded biweekly until the end of the study.

■ ASSOCIATED CONTENT

Supporting Information

The Supporting Information is available free of charge at https://pubs.acs.org/doi/10.1021/acsomega.4c11023.

HDx raw data and SMILES with data (XLSX)

Additional tables, figures, HDX-MS and X-ray crystallography data, molecular dynamics simulations, experimental procedures and reaction schemes for compounds, LC−MS/NMR spectra, chiral purity assessment, assay protocols, and computational chemistry methods (PDF)

■ AUTHOR INFORMATION

Corresponding Authors

Raymond A. Ng − *Olema Oncology, San Francisco 94107 California, United States;* orcid.org/0000-0002-2815-7718; Email: rng@olema.com

David C. Myles − *Olema Oncology, San Francisco 94107 California, United States*; Email: david@olema.com

Authors

Susanna Barratt − *Olema Oncology, San Francisco 94107 California, United States*

Alison Parisian − *Olema Oncology, San Francisco 94107 California, United States*

Gopinath S. Palanisamy − *Olema Oncology, San Francisco 94107 California, United States*

Samiron Phukan − *Aragen Life Sciences Private Ltd., Hyderabad 500076, India;* orcid.org/0000-0002-5009-2340

Richard Sun − *Olema Oncology, San Francisco 94107 California, United States*

Brandon Robello − *Olema Oncology, San Francisco 94107 California, United States*

Guadalupe Peña − *Olema Oncology, San Francisco 94107 California, United States*

Judevin Sapugay − *Olema Oncology, San Francisco 94107 California, United States*

David Yeghikyan − *Olema Oncology, San Francisco 94107 California, United States*

Chenbo Wang − *Olema Oncology, San Francisco 94107 California, United States*

Samir Satish Kher − *Aragen Life Sciences Private Ltd., Hyderabad 500076, India*

Srinivasan Thangathirupathy − *Aragen Life Sciences Private Ltd., Hyderabad 500076, India*

Robert Millikin − *Olema Oncology, San Francisco 94107 California, United States*

Guijun Yu − *Synterys, Inc., Union City 94587 California, United States*

Teruki Watanabe − *Adesis, Inc., New Castle 19720 Delaware, United States*

Fei Zhou − *Adesis, Inc., New Castle 19720 Delaware, United States*

Brian Rich − *Olema Oncology, San Francisco 94107 California, United States*

Alexis Duncan − *Olema Oncology, San Francisco 94107 California, United States*

Samuel E. Andersen − *Olema Oncology, San Francisco 94107 California, United States*

Reena Chawla − *Olema Oncology, San Francisco 94107 California, United States*

David R. Zak − *Department of Cancer Biology, Loyola University Chicago Stritch School of Medicine, Maywood 60153 Illinois, United States*

Dirk A. Heerding − *Olema Oncology, San Francisco 94107 California, United States*

Brian R. Hearn − *Olema Oncology, San Francisco 94107 California, United States*

Geoffrey Greene − *The Ben May Department for Cancer Research, University of Chicago, Chicago 60637 Illinois, United States*

Cyrus L. Harmon − *Olema Oncology, San Francisco 94107 California, United States;* orcid.org/0009-0007-5428-0617

Leslie Hodges-Gallagher − *Olema Oncology, San Francisco 94107 California, United States*

Peter J. Kushner − *Olema Oncology, San Francisco 94107 California, United States*

Sean W. Fanning − *Department of Cancer Biology, Loyola University Chicago Stritch School of Medicine, Maywood 60153 Illinois, United States;* orcid.org/0000-0002-9428-0060

Complete contact information is available at: https://pubs.acs.org/10.1021/acsomega.4c11023

Author Contributions

These authors contributed equally to this work.

Notes

The authors declare the following competing financial interest(s): Raymond A. Ng, Susanna Barratt, Gopinath S. Palanisamy, Brandon Robello, Guadalupe Pea, David Yeghikyan, and David C. Myles are employees of Olema Oncology.

■ ACKNOWLEDGMENTS

The authors gratefully acknowledge Scientific Writers Ltd, UK, for copywriting support. The artwork (Figure 1) was created by Falconieri Visuals, LLC.

ABBREVIATIONS

ADME, absorption, distribution, metabolism, and elimination; antag, antagonist; AP, alkaline phosphatase; AUCinf, area under the concentration−time curve from time 0 extrapolated to infinite time; BCRP, breast cancer resistance protein; Cl_{int}, intrinsic clearance; $cLogD_{7.4}$, calculated distribution coefficient at pH 7.4; C_{max}, maximum serum concentration; Cpd, compound; cyno, cynomolgus monkey; CYP, cytochrome P450; de, diastereomeric excess; DRM, D-ring mimic; ee, enantiomeric excess; hu, human; ID_{50}, half maximal inhibitory dose; LipE, lipophilic efficiency (AP (antag.) pIC_{50}−$cLogD_{7.4}$); mi, mouse; NA, no antagonist activity; NE, no effect; NOE, Nuclear Overhauser Effect; P-gp, p-glycoprotein 1; pIC_{50}, −log IC_{50}; prolif, proliferation; QD, once daily administration; qw, once weekly administration; $T_{1/2}$, half-life; WT, wild-type

REFERENCES

(1) Siegel, R. L.; Miller, K. D.; Wagle, N. S.; Jemal, A. Cancer statistics, 2023. *CA: Cancer J. Clin.* **2023**, *73* (1), 17−48.

(2) https://seer.cancer.gov/statfacts/html/breast-subtypes.html.

(3) (a) Webb, P.; Nguyen, P.; Valentine, C.; Lopez, G. N.; Kwok, G. R.; McInerney, E.; Katzenellenbogen, B. S.; Enmark, E.; Gustafsson, J.; Nilsson, S.; Kushner, P. J. The estrogen receptor enhances AP-1 activity by two distinct mechanisms with different requirements for receptor transactivation functions. *Mol. Endocrinol.* **1999**, *13*, 1672−1685. (b) Berry, M.; Metzger, D.; Chambon, P. Role of the two activating domains of the oestrogen receptor in the cell-type and promoter-context dependent agonistic activity of the anti-oestrogen 4-hydroxytamoxifen. *EMBO J.* **1990**, *9* (9), 2811−2818. (c) Abot, A.; Fontaine, C.; Raymond-Letron, I.; Flouriot, G.; Adlanmerini, M.; Buscata, M.; Otto, C.; Bergès, H.; Laurell, H.; Gourdy, P.; Lenfant, F.; Arnal, J. The AF-1 activation function of estrogen receptor α is necessary and sufficient for uterine epithelial cell proliferation in vivo. *Endocrinology* **2013**, *154* (6), 2222−2233.

(4) Toy, W.; Weir, H.; Razavi, P.; Lawson, M.; Goeppert, A. U.; Mazzola, A. M.; Smith, A.; Wilson, J.; Morrow, C.; Wong, W. L.; De Stanchina, E.; Carlson, K. E.; Martin, T. S.; Uddin, S.; Li, Z.; Fanning, S.; Katzenellenbogen, J. A.; Greene, G.; Baselga, J.; Chandarlapaty, S. Activating *ESR1* mutations differentially affect the efficacy of ER antagonists. *Cancer Discovery* **2017**, *7* (3), 277−287.

(5) (a) Fanning, S. W.; Mayne, C. G.; Dharmarajan, V.; Carlson, K. E.; Martin, T. A.; Novick, S. J.; Toy, W.; Green, B.; Panchamukhi, S.; Katzenellenbogen, B. S.; Tajkhorshid, E.; Griffin, P. R.; Shen, Y.; Chandarlapaty, S.; Katzenellenbogen, J. A.; Greene, G. L. Estrogen receptor alpha somatic mutations Y537S and D538G confer breast cancer endocrine resistance by stabilizing the activating function-2 binding conformation. *eLife* **2016**, *5*, No. e12792. (b) Sharma, A.; Toy, W.; Guillen, V. S.; Sharma, N.; Min, J.; Carlson, K. E.; Mayne, C. G.; Lin, S.; Sabio, M.; Greene, G.; Katzenellenbogen, B. S.; Chandarlapaty, S.; Katzenellenbogen, J. A. Antagonists for constitutively active mutant estrogen receptors: insights into the roles of antiestrogen-core and side-chain. *ACS Chem. Biol.* **2018**, *13*, 3374−3384.

(6) Parisian, A. D.; Barratt, S. A.; Hodges-Gallagher, L.; Ortega, F. R.; Peña, G.; Sapugay, J.; Robello, B.; Sun, R.; Kulp, D.; Palanisamy, G. S.; Myles, D. C.; Kushner, P. J.; Harmon, C. L. Palazestrant (OP-1250), a complete estrogen receptor antagonist, inhibits wild-type and mutant ER-positive breast cancer models as monotherapy and in combination. *Mol. Cancer Ther.* **2024**, *23* (3), 285−300.

(7) Wardell, S. E.; Nelson, E. R.; Chao, C. A.; Alley, H. M.; McDonnell, D. P. Evaluation of the pharmacological activities of RAD1901, a selective estrogen receptor degrader. *Endocr Relat Cancer* **2015**, *22*, 713−724.

(8) Bidard, F.-C.; Kaklamani, V. G.; Neven, P.; Streich, G.; Montero, A. J.; Forget, F.; Mouret-Reynier, M.-A.; Sohn, J. H.; Taylor, D.; Harnden, K. K.; Khong, H.; Kocsis, J.; Dalenc, F.; Dillon, P. M.; Babu, S.; Waters, S.; Deleu, I.; Garcia Saenz, J. A.; Bria, E.; Cazzaniga, M.; Lu, J.; Aftimos, P.; Conlan, M. G.; Bardia, A. Elacestrant (oral selective estrogen receptor degrader) versus standard endocrine therapy for estrogen receptor-positive, human epidermal growth factor receptor 2-negative advanced breast cancer: results from the randomized Phase III EMERALD trial. *J. Clin. Oncol.* **2022**, *40*, 3246−3256.

(9) Osborne, C. K.; Wakeling, A.; Nicholson, R. I. Fulvestrant: an oestrogen receptor antagonist with a novel mechanism of action. *Br. J. Cancer* **2004**, *90*, S2−S6.

(10) Ellis, M. J.; Llombart-Cussac, A.; Feltl, D.; Dewar, J. A.; Jasiowka, M.; Hewson, N.; Rukazenkov, Y.; Robertson, J. F. R. Fulvestrant 500 mg versus anastrozole 1 mg for the first-line treatment of advanced breast cancer: overall survival analysis from the Phase II FIRST study. *J. Clin. Oncol.* **2015**, *33* (32), 3781−3787.

(11) Wardell, S. E.; Yllanes, A. P.; Chao, C. A.; Bae, Y.; Andreano, K. J.; Desautels, T. K.; Heetderks, K. A.; Blitzer, J. T.; Norris, J. D.; McDonnell, D. P. Pharmacokinetic and pharmacodynamic analysis of fulvestrant in preclinical models of breast cancer to assess the importance or its estrogen receptor-α degrader activity in antitumor efficacy. *Breast Cancer Res. Treat* **2020**, *179*, 67−77.

(12) (a) Traboulsi, T.; El Ezzy, M.; Dumeaux, V.; Audemard; Madar, S. Role of SUMOylation in differential ERα transcriptional repression by tamoxifen and fulvestrant in breast cancer cells. *Oncogene* **2019**, *38*, 1019−1037. (b) Vallet, A.; El Ezzy, M.; Diennet, M.; Haidar, S.; Bouvier, M.; Madar, S. The AF-2 cofactor binding region is key for the selective SUMOylation of estrogen receptor alpha by antiestrogens. *J. Biol. Chem.* **2023**, *299* (1), No. 102757.

(13) Wang, L.; Han, T. Pharmacologic induction of ERα SUMOylation disrupts its chromatin binding. *ACS Chem. Biol.* **2024**, *19*, 2383.

(14) Wardell, S. E.; Marks, J. R.; McDonnell, D. P. The turnover of estrogen receptor α by the selective estrogen receptor degrader (SERD) fulvestrant is a saturable process that is not required for antagonist efficacy. *Biochem. Pharmacol.* **2011**, *82* (2), 122−130.

(15) Nawaz, Z.; Lonard, D. M.; Dennis, A. P.; Smith, C. L.; O'Malley, B. W. Proteosome-dependent degradation of the human estrogen receptor. *Proc. Natl. Acad. Sci. U.S.A.* **1999**, *96*, 1858−1862.

(16) De Savi, C.; Bradbury, R. H.; Rabow, A. A.; Norman, R. A.; de Almeida, C.; Andrews, D. M.; Ballard, P.; Buttar, D.; Callis, R. J.; Currie, G. S.; Curwen, J. O.; Davies, C. D.; Donald, C. S.; Feron, L. J. L.; Gingell, H.; Glossop, S. C.; Hayter, B. R.; Hussain, S.; Karoutchi, G.; Lamont, S. G.; MacFaul, P.; Moss, T. A.; Pearson, S. E.; Tonge, M.; Walker, G. E.; Weir, H. M.; Wilson, Z. Optimization of a novel binding motif to (*E*)-3-(3,5-difluoro-4-((1*R*,3*R*)-2-(2-fluoro-2-methylpropyl)-3-methyl-2,3,4,9-tetrahydro-1*H*-pyrido[3,4-b]indol-1-yl)-phenyl)acrylic acid (AZD9496), a potent and orally bioavailable selective estrogen receptor downregulator and antagonist. *J. Med. Chem.* **2015**, *58* (20), 8128−8140.

(17) Scott, J. S.; Moss, T. A.; Balzs, A.; Barlaam, B.; Breed, J.; Carbajo, R. J.; Chiarparin, E.; Davey, P. R. J.; Delpuech, O.; Fawell, S.; Fisher, D. I.; Gagrica, S.; Gangl, E. T.; Grebe, T.; Greenwood, R. D.; Hande, S.; Hatoum-Mokdad, H.; Herlihy, K.; Hughes, S.; Hunt, T. A.; Huynh, H.; Janbon, S. L. M.; Johnson, T.; Kavanagh, S.; Klinowska, T.; Lawson, M.; Lister, A. S.; Marden, S.; McGinnity, D. F.; Morrow, C. J.; Nissink, J. W. M.; O'Donovan, D. H.; Peng, B.; Polanski, R.; Stead, D. S.; Stokes, S.; Thakur, K.; Throner, S. R.; Tucker, M. J.; Varnes, J.; Wang, H.; Wilson, D. M.; Wu, D.; Wu, Y.; Yang, B.; Yang, W. Discovery of AZD9833, a potent and orally bioavailable selective estrogen receptor degrader and antagonist. *J. Med. Chem.* **2020**, *63* (23), 14530−14559.

(18) Liang, J.; Zbieg, J. R.; Blake, R. A.; Chang, J. H.; Daly, S.; DiPasquale, A. G.; Friedman, L. S.; Gelzleichter, T.; Gill, M.; Giltnane, J. M.; Goodacre, S.; Guan, J.; Hartman, S. J.; Ingalla, E. R.; Kategaya, L.; Kiefer, J. R.; Kleinheinz, T.; Labadie, S. S.; Lai, T.; Li, J.; Liao, J.; Liu, Z.; Mody, V.; McLean, N.; Metcalfe, C.; Nannini, M. A.; Oeh, J.; O'Rourke, M. G.; Ortwine, D. F.; Ran, Y.; Ray, N. C.; Roussel, F.; Sambrone, A.; Sampath, D.; Schutt, L. K.; Vinogradova,

https://doi.org/10.1021/acsomega.4c11023
ACS Omega 2025, 10, 22685−22700

M.; Wai, J.; Wang, T.; Wertz, I. E.; White, J. R.; Yeap, S. K.; Young, A.; Zhang, B.; Zheng, X.; Zhou, W.; Zhong, Y.; Wang, Xiaojing GDC-9545 (Giredestrant): A potent and orally bioavailable selective estrogen receptor antagonist and degrader with an exceptional preclinical profile for ER+ breast cancer. *J. Med. Chem.* **2021**, *64* (16), 11841−11856.

(19) Kahraman, M.; Govek, S. P.; Nagasawa, J. Y.; Lai, A.; Bonnefous, C.; Douglas, K.; Sensintaffar, J.; Liu, N.; Lee, K.; Aparicio, A.; Kaufman, J.; Qian, J.; Shao, G.; Prudente, R.; Joseph, J. D.; Darimont, B.; Brigham, D.; Heyman, R.; Rix, P. J.; Hager, J. H.; Smith, N. D. Maximizing ER-α degradation maximizes activity in a tamoxifen-resistant breast cancer model: identification of GDC-0927. *ACS Med. Chem. Lett.* **2019**, *10*, 50−55.

(20) Bhagwat, S. V.; Zhao, B.; Shen, W.; Mur, C.; Barr, R.; Kindler, L. J.; Rubio, A.; Bastian, J. A.; Cohen, J. D.; Mattioni, B. E.; Yuen, E.; Baker, T. K.; Castanares, M. A.; Fei, D.; Manro, J. R.; Lallena, M. J.; Peng, S.-B.; de Dios, A. Abstract 1236: preclinical characterization of LY3484356, a novel, potent and orally bioavailable selective estrogen receptor degrader (SERD). *Cancer Res.* **2021**, *81*, 1236−1236.

(21) (a) El-Ahmad, Y.; Tabart, M.; Halley, F.; Certal, V.; Thompson, F.; Filoche-Romme, B.; Gruss-Leleu, F.; Muller, C.; Brollo, M.; Fabien, L.; Loyau, V.; Bertin, L.; Richepin, P.; Pilorge, F.; Desmazeau, P.; Girardet, C.; Beccari, S.; Louboutin, A.; Lebourg, G.; Le-Roux, J.; Terrier, C.; Vallee, F.; Steier, V.; Mathieu, M.; Rak, A.; Abecassis, P.-Y.; Vicat, P.; Benard, T.; Bouaboula, M.; Sun, F.; Shomali, M.; Hebert, A.; Levit, M.; Cheng, H.; Courjaud, A.; Ginesty, C.; Perrault, C.; Garcia-Echeverria, C.; McCort, G.; Schio, L. Discovery of 6-(2,4-dichlorophenyl)-5-[4-[(3*S*)-1-(3-fluoropropyl)pyrrolidin-3-yl]-oxyphenyl]-8,9-dihydro-7*H*-benzo[7]annulene-2-carboxylic acid (SAR439859), a potent and selective estrogen receptor degrader (SERD) for the treatment of estrogen-receptor-positive breast cancer. *J. Med. Chem.* **2020**, *63* (2), 512−528. (b) El-Ahmad, Y.; Croq, V.; Wehrey, C.; Shomali, M; Schio, L. Chapter 7: Discovery and chemical development of amcenestrant: an oral selective estrogen receptor degrader (SERD) for the treatment of estrogen receptor positive breast cancer. In *Complete Accounts of Integrated Drug Discovery and Development: Recent Examples from the Pharmaceutical Industry*, Pesti, J. A.; Abdel-Magid, A. F.; Vaidyanathan, R.., (Eds.), ACS Symposium Series; American Chemical Society: Washington, DC, 2022; Vol. *4*, pp 275−300.

(22) Gough, S. M.; Flanagan, J. J.; Teh, J.; Andreoli, M.; Rousseau, E.; Pannone, M.; Bookbinder, M.; Willard, R.; Davenport, K.; Bortolon, E.; Cadelina, G.; Gordon, D.; Pizzano, J.; Macaluso, J.; Soto, L.; Corradi, J.; Digianantonio, K.; Drulyte, I.; Morgan, A.; Quinn, C.; Bekes, M.; Ferraro, C.; Chen, X.; Wang, G.; Dong, H.; Wang, J.; Langley, D. R.; Houston, J.; Gedrich, R.; Taylor, I. C. Oral estrogen PROTAC vepdegestrant (ARV-471) is highly efficacious as monotherapy an in combination with CDK4/6 or PI3K/mTOR pathway inhibitors in preclinical ER+ breast cancer models. *Clin. Cancer Res.* **2024**, *30* (16), 3549−3563.

(23) Neupane, N.; Bawek, S.; Gurusinghe, S.; Ghaffary, E. M.; Mirmosayyeb, O.; Thapa, S.; Falkson, C.; O'Regan, R.; Dhakal, A. Oral SERD, a novel endocrine therapy for estrogen receptor-positive breast cancer. *Cancers (Basel)* **2024**, *16* (3), 619.

(24) Watt, A. C.; Goel, S. Cellular mechanisms underlying response and resistance to CDK4/6 inhibitors in the treatment of hormone receptor-positive breast cancer. *Breast Cancer Res.* **2022**, *24* (1), 17.

(25) (a) Lu, Y.-S.; Im, S.; Colleoni, M.; Franke, F.; Bardia, A.; Cardoso, F.; Harbeck, N.; Hurvitz, S.; Chow, L.; Sohn, J.; Lee, K. S.; Campos-Gomez, S.; Vazquez, R. V.; Jung, K. H.; Babu, K. G.; Wheatley-Price, P.; De Laurentiis, M.; Im, Y.-H.; Kuemmel, S.; El-Saghir, N.; O-Regan, R.; Gasch, C.; Solovieff, N.; Wang, C.; Wang, Y.; Chakravartty, A.; Ji, Y.; Tripathy, D. Updated overall survival of ribociclib plus endocrine therapy versus endocrine therapy alone in pre- and perimenopausal patients with HR+/Her2- advanced breast cancer in MONALEESA-7: a Phase III randomized clinical trial. *Clin. Cancer Res.* **2022**, *28* (5), 851−859. (b) Neven, P.; Fasching, P. A.; Chia, S.; Jerusalem, G.; De Laurentiis, M.; Im, S.-A.; Petrakova, K.; Bianchi, G. V.; Martin, M.; Nusch, A.; Sonke, G. S.; De la Cruz-Merino, L.; Beck, J. T.; Zarate, J. P.; Wang, Y.; Chakravartty, A.; Wang, C.; Slamon, D. J. Updated overall survival from the MONALEESA-3 trial in postmenopausal women with HR+/HER2- advanced breast cancer receiving first-line ribociclib plus fulvestrant. *Breast Cancer Res.* **2023**, *25*, 103.

(26) Onesti, C. E.; Jerusalem, G. CDK4/6 inhibitors in breast cancer: differences in toxicity profiles and impact on agent choice. A systematic review and meta-analysis. *Exp. Rev. Anticancer Ther.* **2021**, *21* (3), 283−298.

(27) (a) Sakamoto, T.; Eguchi, H.; Omoto, Y.; Ayabe, T.; Mori, H.; Hayashi, S. Estrogen recepto-mediated effects of tamoxifen on human endometrial cancer cells. *Mol. Cell. Endocrinol.* **2002**, *192*, 93−104. (b) Littlefield, B. A.; Gurpide, E.; Markiewicz, L.; McKinley, B.; Hochberg, R. B. A simple and sensitive microliter plate estrogen bioassay based on stimulation of alkaline phosphatase in Ishikawa cells: estogenic action of D5 adrenal steroids. *Endocrinology* **1990**, *127*, 2757−2762.

(28) (a) Wijayaratne, A. L.; McDonnell, D. P. The human estrogen receptor-*a* is a ubiquitinated protein whose stability is affected differentially by agonists, antagonists, and selective estrogen receptor modulators. *J. Biol. Chem.* **2001**, *276* (38), 35684. (b) Guan, J.; Zhou, W.; Hafner, M.; Blake, R. A.; Chalouni, C.; Chen, I. P.; De Bruyn, T.; Giltnane, J. M.; Hartman, S. J.; Heidersbach, A.; Houtman, R.; Ingalla, E.; Kategaya, L.; Kleinheinz, T.; Li, J.; Martin, S. E.; Modrusan, Z.; Nannini, M.; Oeh, J.; Ubhayakar, S.; Wang, X.; Wertz, I. E.; Young, A.; Yu, M.; Sampath, D.; Hager, J. H.; Friedman, L. S.; Daemen, A.; Metcalfe, C. Therapeutic ligands antagonize estrogen receptor function by impairing its mobility. *Cell* **2019**, *178*, 949−963.

(29) McSwiggen, D. T.; Liu, H.; Tan, R.; Puig, S. A.; Akella, L. B.; Berman, R.; Bretan, M.; Chen, H.; Darzacq, X.; Ford, K.; Godbey, R.; Gonzalez, E.; Hanuka, A.; Heckert, A.; Ho, J. J.; Johnson, S. L.; Kelso, R.; Klammer, A.; Krishnamurthy, R.; Li, J.; Lin, K.; Margolin, B.; McNamara, P.; Meyer, L.; Pierce, S. E.; Sule, A.; Stashko, C.; Tang, Y.; Anderson, D. J.; Beck, H. P. A high-throughput platform for single-molecule tracking identifies drug interaction and cellular mechanisms. *eLife* **2023**, *12*, RP93183.

(30) Fanning, S. W.; Hodges-Gallagher, L.; Myles, D. C.; Sun, R.; Fowler, C. E.; Plant, I. N.; Green, B. D.; Harmon, C. L.; Greene, G. L.; Kushner, P. J. Specific stereochemistry of OP-1074 disrupts estrogen receptor alpha helix 12 and confers pure antiestrogenic activity. *Nat. Commun.* **2018**, *9*, 2368.

(31) Kushner, P. J.; Myles, D. C.; Harmon, C. L.; Hodges-Gallagher, L. C. Anti-estrogenic compounds. US 2016/0311805 A1, 2016.

(32) Anstead, G. M.; Carlson, K. E.; Katzenellenbogen, J. A. The estradiol pharmacophore: Ligand structure-estrogen receptor binding affinity relationships and a model for the receptor binding site. *Steroids* **1997**, *62*, 268−303.

(33) Zbieg, J. R.; Liang, J.; Li, J.; Blake, R. A.; Chang, J.; Friedman, L.; Goodacre, S.; Hartman, S. J.; Ingalla, E. R.; Kiefer, J. R.; Kleinheinz, T.; Labadie, S.; Lai, T.; Liao, J.; McLean, N.; Metcalfe, C.; Mody, V.; Nannini, M.; Ortwine, D. F.; Ran, Y.; Ray, N.; Roussel, F.; Sambrone, A.; Sampath, D.; Vinogradova, M.; Wai, J.; Wang, T.; Yeap, K.; Zhang, B.; Zheng, X.; Zhong, Y.; Wang, X. Discovery of GNE-502 as an orally bioavailable and potent degrader for estrogen receptor positive breast cancer. *Bioorg. Med. Chem. Lett.* **2021**, *50*, No. 128335.

(34) Although we started our investigation prior to Genentech and delayed publication of our results, compound was disclosed by Astra Zeneca. Scott, J. S.; Breed, J.; Carbajo, R. J.; Davey, P. R.; Greenwood, R.; Huynh, H. K.; Klinowska, T.; Morrow, C. J.; Moss, T. A.; Polanski, R.; Nissink, J. W. M.; Varnes, J.; Yang, B. Building bridges in a series of estrogen receptor degraders: an application of metathesis in medicinal chemistry. *ACS Med. Chem. Lett.* **2019**, *10*, 1492−1497.

(35) Compounds **30** and **32** were disclosed previously by Genentech.(a) Liang, J.; Blake, R.; Chang, J.; Friedman, L. S.; Goodacre, S.; Hartman, S.; Ingalla, E. R.; Kiefer, J. R.; Kleinheinz, T.; Labadie, S.; Li, J.; Lai, K. W.; Liao, J.; Mody, V.; McLean, N.; Metcalfe, C.; Nannini, M.; Otwine, D.; Ran, Y.; Ray, N.; Roussel, F.; Sambrone, A.; Sampath, D.; Vinogradova, M.; Wai, J.; Wang, T.;

https://doi.org/10.1021/acsomega.4c11023
ACS Omega 2025, 10, 22685−22700

Yeap, K.; Young, A.; Zbieg, J.; Zhang, B.; Zheng, X.; Zhong, Y.; Wang, X. Discovery of GNE-149 as a full antagonist and efficient degrader of estrogen receptor alpha for ER+ breast cancer. *ACS Med. Chem. Lett.* **2020**, *11*, 1342−1347; Compounds **23** and **26** was also previously disclosed by Genentech. (b) Goodacre, S. C.; Labadie, S.; Liang, J.; Ortwine, D. F.; Ray, N. C.; Wang, X.; Zbieg, J.; Zhang, B. Tetrahydropyrido[3,4-b]indole estrogen receptor modulators and uses thereof. WO 2016/097072 A1, 2016.

(36) Tan, Q.; Blizzard, T. A.; Morgan, J. D., II; Birzin, E. T.; Chan, W.; Yang, Y. T.; Pai, L.; Hayes, E. C.; DaSilva, C. A.; Warrier, S.; Yudkovitz, J.; Wilkinson, H. A.; Sharma, N.; Fitzgerald, P. M. D.; Li, S.; Colwell, L.; Fisher, J. E.; Adamski, S.; Reszka, A. A.; Kimmel, D.; DiNinno, F.; Rohrer, S. P.; Freedman, L. P.; Schaeffer, J. M.; Hammond, M. L. Estrogen receptor ligands. Part 10: Chromanes: old scaffolds for new SERAMs. *Bioorg. Med. Chem. Lett.* **2005**, *15*, 1675−1681.

(37) Luo, S.-X.; Liu, Y.; Lambrecht, M. J.; Ortwine, D. F.; DiPasquale, A. G.; Liang, J.; Wang, X.; Zbeig, J. R.; Li, Jun *cis*-Selective synthesis of 1,3-disubstituted tetrahydro-β-carbolines from *N*-sulfonyl *N*,*S*-acetals. *Org. Biomol. Chem.* **2019**, *17*, 9510−9513.

(38) (a) Cox, E. D.; Cook, J. M. The Pictet-Spengler condensation: a new direction for an old reaction. *Chem. Rev.* **1995**, *95*, 1797−1842. (b) Ungemach, F.; DiPierro, M.; Weber, R.; Cook, J. M. Stereospecific synthesis of *trans*-1,3-disubstituted-1,2,3,4-tetrahydro-β-carbolines. *J. Org. Chem.* **1981**, *46*, 164−168.

(39) Shiau, A. K.; Barstad, D.; Loria, P. M.; Cheng, L.; Kushner, P. J.; Agard, D. A.; Greene, G. L. The structural basis of estrogen receptor/coactivator recognition and the antagonism of this interaction by tamoxifen. *Cell* **1998**, *95* (7), 927−937.

(40) Nettles, K. W.; Greene, G. L. Nuclear receptor ligands and cofactor recruitment: Is there a coactivator "on deck"? *Mol. Cell* **2003**, *11* (4), 850−851.

(41) Pike, A. C. W.; Brzozowski, A. M.; Walton, J.; Hubbard, R. E.; Thorsell, A.-G.; Li, Y.-L.; Gustafsson, J.-A.; Carlquist, M. Structural insights into the mode of action of a pure antiestrogen. *Structure* **2001**, *9*, 145−153.

(42) Maximov, P. Y.; Abderrahman, B.; Fanning, S. W.; Sengupta, S.; Fan, P.; Curpan, R. F.; Rincon, D. M. Q.; Greenland, J. A.; Rajan, S. S.; Greene, G. L.; Jordan, V. C. Endoxifen, 4-hydroxytamoxifen and an estrogenic derivative modulate estrogen receptor complex mediated apoptosis in breast cancer. *Mol. Pharmacol.* **2018**, *94* (2), 812−822.

(43) Horn, J. R.; Kraybill, B.; Petro, E. J.; Coales, S. J.; Morrow, J. A.; Hamuro, Y.; Kossiakoff, A. A. The role of protein dynamics in increasing binding affinity for an engineered protein-protein interaction established by H/D exchange mass spectrometry. *Biochemistry* **2006**, *45* (28), 8488−8498.

(44) Fanning, S. W.; Jeselsohn, R.; Dharmarajan, V.; Mayne, C. G.; Karimi, M.; Buchwalter, G.; Houtman, R.; Toy, W.; Fowler, C. E.; Han, R.; Lainé, M.; Carlson, K. E.; Martin, T. A.; Nowak, J.; Nwachukwu, J. C.; Hosfield, D. J.; Chandarlapaty, S.; Tajkhorshid, E.; Nettles, K. W.; Griffin, P. R.; Shen, Y.; Katzenellenbogen, J. A.; Brown, M.; Greene, G. L. The SERM/SERD bazedoxifene disrupts ESR1 helix 12 to overcome acquired hormone resistance in breast cancer cells. *eLife* **2018**, *7*, No. e37161.

(45) Wick, M. J.; Diaz, A.; Thomas, M.; Moriarty, A. D.; Quinn, M.; Guerra, M.; Zhu, P.; Smith, P.; Tolcher, A. W.; Puyang, X.; Patnaik, A.; Korpal, M.; Rasco, D.; Papadopoulos, K. P. Establishment and characterization of ST941/C; an ESR1-mutant ER+ breast cancer cell line and xenograft from a patient with acquired resistance to endocrine therapy. *Cancer Res.* **2017**, *77*, P3-04-26.

https://doi.org/10.1021/acsomega.4c11023
ACS Omega 2025, 10, 22685−22700